CORROSION BEHAVIOUR OF COPPER ALLOYS IN GASEOUS URANIUM HEXAFLUORIDE

by

S W VORSTER

CORROSION BEHAVIOUR OF COPPER ALLOYS IN GASEOUS URANIUM HEXAFLUORIDE

Schalk Willem Vorster

A Dissertation Submitted to the Faculty of Engineering, University of the Witwatersrand, Johannesburg, for the degree of Master of Science in Engineering.

1978

DECLARATION

I, SCHALK WILLEM VORSTER, declare that this dissertation is my own work and has not been submitted for a degree in any other university.

S.W. Vorster

ACKNOWLEDGEMENTS

Thanks are due to Dr. W.L. Grant for permission to submit this dissertation.

The author further wishes to thank professor F.P.A. Robinson for his guidance, Dr. C.M. van der Walt and Dr. I.A. Kotzé for valuable assistance in obtaining X-ray and electron spectrometric data and Mr. E.C. Kelly for his assistance in the experimental part of the investigation.

Finally I would like to thank Mrs. M.E. Reynecke for typing the dissertation.

A B S T R A C T

The corrosion behaviour of nineteen copper alloys in gaseous uranium hexafluoride at a pressure of 15 kPa, was investigated. Corrosion/time relationships were established for five temperatures ranging from 50 to 150 ^{o}C and for exposure times between 5 and 1 000 h. Post-corrosion test studies were performed, employing a variety of physical techniques, including X-ray diffraction and X-ray fluorescence analysis, electron spectroscopy and electron microscopy.

Electrolytic copper, beryllium copper, aluminium bronze and 5 % phosphor bronze were found to be the most resistant of the alloys investigated. The copper-zinc and copper-zinc-tin alloys suffered dezincification.

Corrosion activation energies were comparatively low, ranging from 12,8 to 54 kJ mol^{-1}.

The uranium-containing corrosion products found, generally differed from those predicted by the Agron diagram, the more reactive alloys giving rise to U_2F_9 at much lower temperatures than expected.

Both mild prefluorination with UF_6 (50 ^{o}C, 140 h exposure) and mild oxidation (150 ^{o}C, 15 min.) enhanced the resistance to UF_6 attack.

TABLE OF CONTENTS

(v) 3. ...

1. URANIUM HEXAFLUORIDE : A SURVEY OF ITS MOST IMPORTANT PHYSICAL AND CHEMICAL PROPERTIES

1.1 Introduction

Uranium hexafluoride is by far the most volatile uranium compound and, therefore it is used extensively in all processes for the enrichment of uranium. It was discovered in 1909 by Ruff and Heinzelmann [1] who prepared it by the reaction of fluorine with uranium metal or uranium carbide. The compound received little attention until the second world war when the gaseous diffusion process was developed. The entire research effort in the wartime period was directed towards short-term military ends, with the result that, although a large number of physical constants were determined and some chemical properties were studied, the descriptive chemistry did not receive much attention. In 1968 Brown [2] wrote : "Although the physical properties of the hexafluorides, particularly those of UF_6, have been investigated in some detail, their chemical behaviour has been relatively little studied." This remark may be extended to include corrosion processes, for, although some declassified research work was published, especially by the French during the period 1961 to 1969, it rarely elucidated corrosion reaction mechanisms.

1.2 Physical Properties of Uranium Hexafluoride

The most important physical properties of uranium hexafluoride are summarized in table 1.1. Of great practical importance

---

1) O. Ruff and A. Heinzelmann, Z. Anorg. Chem. 72, 63-84 (1911)

2) D. Brown, "Halides of the Lanthanides and Actinides," Wiley-Interscience (1968), p.27

is the remarkably high vapour pressure at room temperature (15,7 kPa). The phase diagram is shown in figure 1.1, from which it can be seen that the sublimation temperature of UF_6 is 56,54 °C and the triple point 64,02 °C (at 149,7 kPa).

1.3 Chemical Properties of Uranium Fluorides

Some of the chemical properties of uranium hexafluoride which are relevant to a corrosion study involving this material, will now be reviewed.

1.3.1 The intermediate uranium fluorides

Most of the descriptive chemistry of uranium hexafluoride originated in the Manhattan project and frequently concerned the reduction of UF_6 to UF_4, or to one of the "intermediate fluorides" (α-UF_5, β-UF_5, U_2F_9 and U_4F_{17}). The existence of uranium fluorides at a uranium valence intermediate between 4 and 6 under various conditions of temperature and pressure has been demonstrated by Agron [3], Broadley and Longton [4], Labaton [5] and others. Nguyen-Hoang-Nghi [6] reported the existence of yet another intermediate fluoride, U_5F_{22}, which forms at low temperatures.

The relationships between UF_6 and UF_4 and the abovementioned intermediate fluorides are conveniently summarized in the so-called Agron diagram, shown in figure 1.2. This diagram has been verified

---

3) P. Agron, AECD-1878 (1948)

4) J.S. Broadly and P.B. Longton, U.K.A.E.A.-RDR-Tech. note 60

5) V.Y. Labaton, U.K.A.E.A. No. IGR-RKA 193 (1956)

6) Nguyen-Hoang-Nghi, CEA 1976 (1961)

by several workers, notably by Nguyen-Hoang-Nghi and by Barberi and Hartmanshenn [7], using a microcalorimetric technique.

It was found that uranium hexafluoride reacts with uranium tetrafluoride in a stepwise manner, yielding U_4F_{17}, U_2F_9, α-UF_5 or β-UF_5, depending on the hexafluoride pressure and the temperature of the system. The rate at which equilibrium is obtained depends on the nature of the tetrafluoride. The following reactions represent the essential steps in attaining equilibrium :

$$3\,\alpha\,UF_5(s) \gtrless U_2F_9(s) + UF_6(g)$$

$$3\,\beta\,UF_5(s) \gtrless U_2F_9(s) + UF_6(g)$$

$$7/2\;U_2F_9(s) \gtrless 3/2\;U_4F_{17}(s) + UF_6(g)$$

$$2\;U_4F_{17}(s) \gtrless 7\;UF_4(s) + UF_6(g)$$

In each of the above equations the equilibrium constant is k_p.

$$\frac{d\ \ln\ k_p}{dT} = \Delta H / RT^2 \quad \text{(van 't Hoff equation)}$$

(where T = absolute temperature, R = gas constant and H = heat of the reaction). The Agron diagram can therefore be derived.

Uranium pentafluoride (the colour of which somehow depends on the preparation method) is normally a white substance and exists in two forms of which β-UF_5 is the low temperature and α-UF_5 the high temperature variation. The melting point of UF_5 has been given [2] as 346 ^{o}C, under a

---

7) P. Barberi and O. Hartmanshenn, CEA-N-916

pressure of UF_6 greater than 160 kPa, since at lower pressures U_2F_9 and U_4F_{17} are successively formed. Zachariasen [8] obtained powder diffraction patterns from both α- and β-UF_5 sealed in thin-walled glass capillaries. α-UF_5 is tetragonal body-centered with a_1 = 0,653 nm and a_3 = 0,447 nm with two stoichiometric molecules per unit cell. β-UF_5 is also tetragonal body-centered with a unit cell containing eight stoichiometric molecules and with dimensions a_1 = 1,147 nm and a_3 = 0,521 nm. The interatomic distances are

α-UF_5, U-F = 0,220 nm.

β-UF_5, U-F = 0,223 nm.

Zachariasen rejects the chemical formula $UF_4 . UF_6$ for UF_5 and points out that the uranium atoms are all equivalent in the structure.

The chemical properties of the intermediate fluorides have not been very well investigated. β-UF_5 is rapidly hydrolyzed in the presence of traces of water. This usually leads to destruction of its crystallinity and consequently X-ray identification is thereby thwarted :

$$2\ UF_5 + 2\ H_2O \longrightarrow UO_2F_2 + UF_4 + 4\ HF$$

In moist air α-UF_5 appears to be more susceptible to hydrolysis than β-UF_5.[9]

β-UF_5 can be converted to α-UF_5 by raising the temperature. This reaction is irreversible. [7]

---

8) W.H. Zachariasen, Acta Cryst. 2, 296 (1949)

9) J.J. Katz and E. Rabinowitch,"The Chemistry of Uranium The Element, Its Binary and Related Compounds," Dover Publications, Inc. (1951)

U_2F_9 (diuranium enneafluoride) was discovered in the course of a study of the UF_4 (s) + UF_6(g) reaction and was initially referred to as "black fluoride" or "black UF_4" as it was thought to be a crystal modification of UF_4. Agron et al.[10] elucidated its structure by means of X-ray diffraction. A similar substance was encountered by British workers in the course of corrosion studies on mild steel.[9] Samples exposed to UF_6 vapour formed a black scale with the composition $FeF_2.2UF_5$ (or $FeF_3.U_2F_9$).

U_2F_9 has a cubic structure with a_0 = 0,84538 ± 0,0001 nm. The unit cell contains eight molecules with a calculated density of 7060 kg m^{-3}. The uranium atoms are all structurally equivalent. The formulas $UF_4 . UF_5$ or $3\,UF_4 . UF_6$, which indicate the presence of two kinds of uranium atoms, are therefore inadmissible. The substance may be regarded as a mixed crystal with rational proportions in which resonance renders all the uranium atoms equivalent.[9]

$$\left(U^{4+}_{0,5} + U^{5+}_{0,5} F_{4,5}\right) \text{ or } \left(U^{4+}_{0,75} + U^{6+}_{0,25} F_{4,5}\right)$$

This resonance may explain the dark colour of the substance. U_2F_9 is much less readily hydrolysed in moist air than UF_5.

U_4F_{17} was found by Agron et al [10] by means of chemical and X-ray analysis. The reaction between UF_6 and UF_4 at higher temperatures (250 - 325 °C) gave rise to a product, the X-ray pattern of which resembled that of UF_4, but "extraneous" lines were also

---

10) P. Agron, A Grenall, R. Kurim & S. Weller, MDDC-1588 (1948) (1210)

observed. The samples yielding this pattern were described as "distorted UF_4". Chemical analysis of U^{IV}, F and total U of several samples of "distorted UF_4" showed that the composition lay close to halfway between UF_4 and U_2F_9 and it was assigned the formula U_4F_{17}. The crystal structure of U_4F_{17} is not known. Its density is 6940 kg m^{-3}. [9]

U_5F_{22} was found as the reaction product when UF_6 reacts with UF_4 in the temperature region 20 - 45 °C. Contrary to the results by Nghi [6], Barberi and Hartmanshenn [7] found that the final product of the UF_4-UF_6 reaction at 26 °C is β-UF_5.

1.3.2 Selected chemical properties of uranium hexafluoride

UF_6 must be considered a moderately strong fluorinating agent. It is the least reactive of the actinide hexafluorides, but as is the case with almost all fluorides, two reactions are vigorous. These are the hydrolysis reaction and the reaction with hydrocarbons, leading to the general belief that UF_6 is a very reactive compound. This is not generally true but must be viewed against the very stringent requirements of the enrichment industry. It is found, for instance, that corrosion rates of some engineering materials in uranium hexafluoride are orders of magnitude lower than rates experienced with ordinary river water. Yet, the corrosion of metals by UF_6 is of prime importance in the selection of construction materials for an enrichment plant. The chemical and physical nature of UF_6 (e.g. its destruction by moisture and its toxicity) necessitates unique precautions to eli-

minate all unwanted reactions. Chemically clean surfaces and a high level of vacuum tightness are required of all vessels and pipes carrying UF_6. Not only does corrosion lead to the loss of valuable UF_6, but the creation of "dust" in the form of corrosion products can lead to serious impairment of plant performance.

Laboratory investigations involving UF_6 are complicated considerably by the nature of the gas. Unwanted reactions are sometimestriggered by impurities present in concentrations of parts per million. Experimentation (including corrosion studies) therefore has to be carried out under conditions of extreme cleanliness.

The following chemical properties of UF_6 are relevant :

1. UF_6 easily sheds one or more fluorine atoms to form a family of subfluorides such as α- and β-UF_5, U_2F_9 , U_4F_{17} and UF_4 as already described. These subfluorides are frequently found in corrosion layers.

2. UF_6 will react violently with organic materials. A notable exception is found in fully fluorinated polymers, such as polytetrafluoro-ethylene.

3. UF_6 is easily decomposed by water, the final endproduct being determined by the relative excess of UF_6 and H_2O e.g. UO_2F_2, $U_3O_5F_8$, $U_2O_3F_6$ or UOF_4. Complex compounds such as $UO_2F_2.H_2O$ and $UO_2F_2.H_2O.HF$ with different relative numbers of molecules are frequently encountered.

From the reaction

$$UF_6 + 2\ H_2O \longrightarrow UO_2F_2 + 4\ HF$$

it follows that one gram of water leads to the loss of of ten grams of UF_6.

4. The use of glass apparatus is restricted by the following chain reaction :

$$UF_6 + 2\ H_2O \longrightarrow UO_2F_2 + 4\ HF$$

$$SiO_2 + 4\ HF \longrightarrow SiF_4 + 2\ H_2O$$

As water is recycled it follows that total loss of UF_6 results, unless the glass surface can be totally dehydrated and all initial HF removed from the UF_6. In practice neither of these requirements is easily complied with.

5. UF_6 reacts with most industrially important metals. This aspect will be discussed in Chapter II.

TABLE 1.1 : SOME PHYSICAL PROPERTIES AND SELECTED PHYSICAL CONSTANTS FOR URANIUM HEXAFLUORIDE

Colour of solid		white
Colour of vapour		colourless
Triple point		64,02 ^{o}C
Boiling point		56,54 ^{o}C
Vapour pressure at 0 ^{o}C		2,32 kPa
Vapour pressure at 25 ^{o}C		15,72 kPa
Vapour pressure at triple point		149,95 kPa
Critical temperature		230,2 ^{o}C
Critical pressure		4,55 MPa
Density, solid	(25 ^{o}C)	5060 kg m^{-3}
Density, liquid	(70 ^{o}C)	3595 kg m^{-3}
Viscosity, liquid	(70 ^{o}C)	0,91 MPa.s
Viscosity, gas	(80 ^{o}C)	19,- µPa.s
Surface tension	(70 ^{o}C)	1,68 Pa
Dielectric constant, gas	(67 ^{o}C)	1,00929
Thermal conductivity, gas	(5 ^{o}C)	0,42 $Js^{-1}m^{-2}\ {}^{o}C^{-1}$

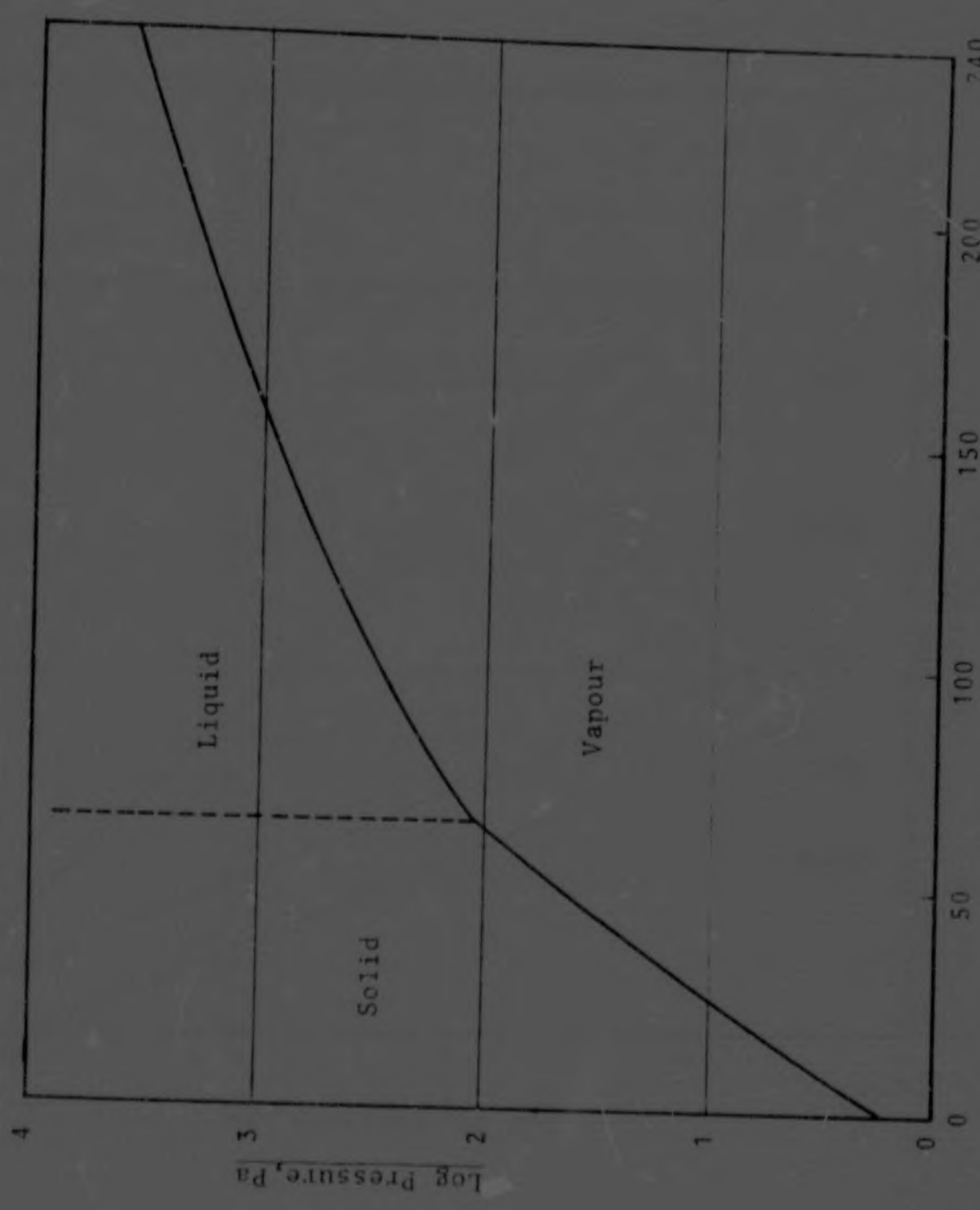

FIGURE 1.1 : UF_6-PHASE DIAGRAM[11]

---

11) R. DeWitt, "Uranium Hexafluoride: A Survey of the Physico-chemical Properties", (Report GAT - 28; Goodyear Atomic Corporation, August 1960).

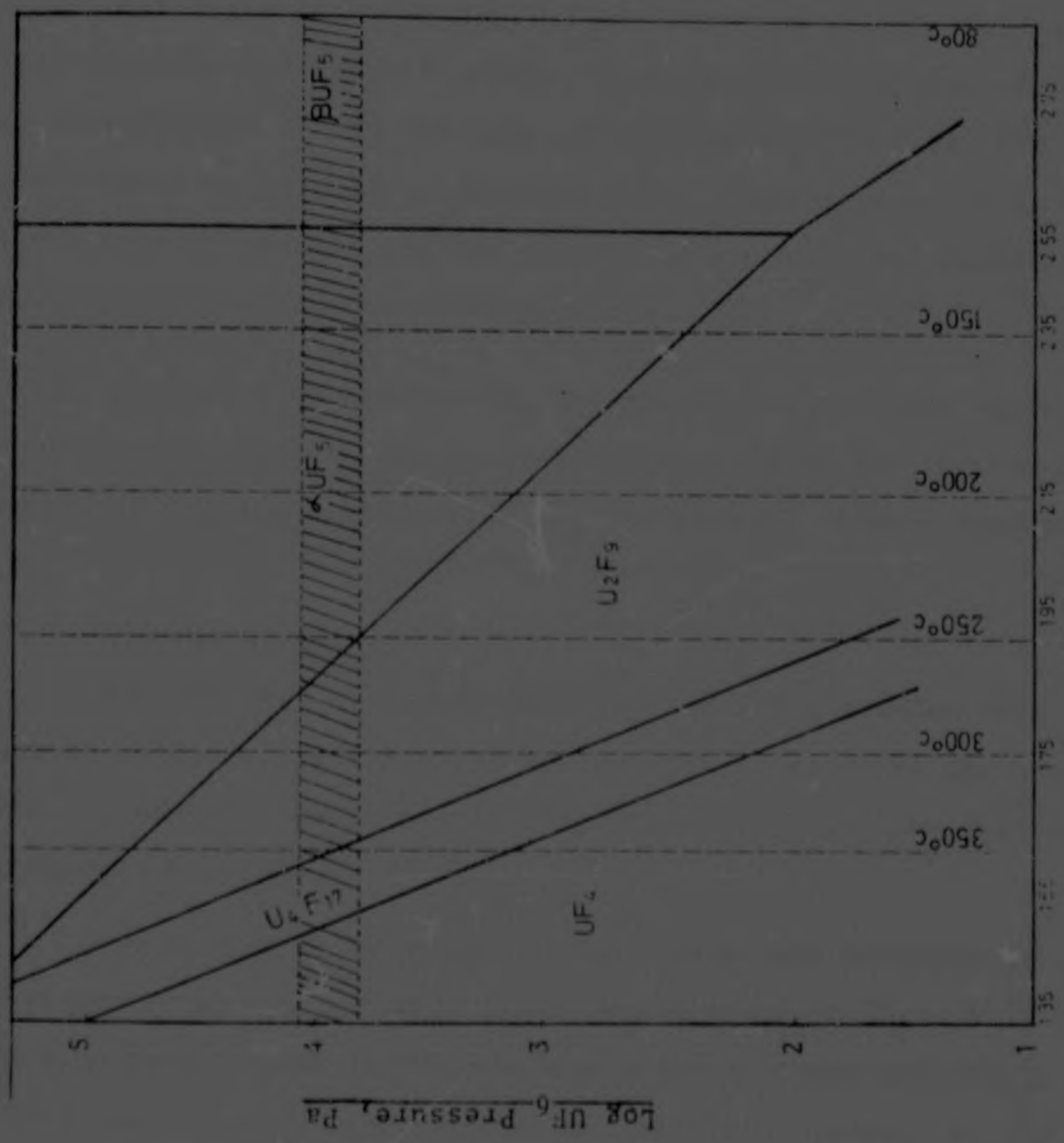

FIGURE 1.2 : AGRON DIAGRAM (Pressure range for present investigation indicated)

2. CORROSION OF METALS AND ALLOYS IN URANIUM HEXAFLUORIDE - A LITERATURE SURVEY

2.1 Introduction

Corrosion has been defined as ".... the destruction of a metal or alloy by chemical change, electrochemical change or physical dissolution." [1] In the case of uranium hexafluoride, the attack on the metal is normally relatively mild, and the emphasis is more on the loss of process gas and the subsequent problems caused by minute quantities of corrosion products.

The reaction between UF_6 and metals has many analogies with dry oxidation. Matters are, however, complicated by the special properties of uranium hexafluoride and the lack of certain fundamental data.

2.2 Literature Survey

Much of the corrosion research concerning uranium hexafluoride is classified. A brief review will be given of the unclassified literature, which mostly originated from the Commissariat à l'Energie Atomique.

A publication by Heymann and Kelling [2] gives some information on the rate of penetration of a variety of alloys exposed to 240 kPa UF_6 at 80 °C (see table 2.1). The difference in behaviour between the two copper-zinc alloys studied was related to the nickel and aluminium content of the less resistant alloy. Large numbers of black, dark brown, light brown, yellow and colourless crystals were observed on the samples

---

1) U.R. Evans, The Corrosion and Oxidation of Metals : Scientific Principles and Practical Applications, Edward Arnold (1961) p.2

2) D. Heymann and F.E.T. Kelling, Corrosion Technology, 5, 148-151, (1958)

2. CORROSION OF METALS AND ALLOYS IN URANIUM HEXAFLUORIDE - A LITERATURE SURVEY

2.1 Introduction

Corrosion has been defined as ".... the destruction of a metal or alloy by chemical change, electrochemical change or physical dissolution." [1] In the case of uranium hexafluoride, the attack on the metal is normally relatively mild, and the emphasis is more on the loss of process gas and the subsequent problems caused by minute quantities of corrosion products.

The reaction between UF_6 and metals has many analogies with dry oxidation. Matters are, however, complicated by the special properties of uranium hexafluoride and the lack of certain fundamental data.

2.2 Literature Survey

Much of the corrosion research concerning uranium hexafluoride is classified. A brief review will be given of the unclassified literature, which mostly originated from the Commissariat à l'Energie Atomique.

A publication by Heymann and Kelling [2] gives some information on the rate of penetration of a variety of alloys exposed to 240 kPa UF_6 at 80 °C (see table 2.1). The difference in behaviour between the two copper-zinc alloys studied was related to the nickel and aluminium content of the less resistant alloy. Large numbers of black, dark brown, light brown, yellow and colourless crystals were observed on the samples

---

1) U.R. Evans, The Corrosion and Oxidation of Metals : Scientific Principles and Practical Applications, Edward Arnold (1961) p.2

2) D. Heymann and F.E.T. Kelling, Corrosion Technology, 5, 148-151, (1958)

after exposure to UF_6. No effort was made to identify these crystals. A simple method, based on measuring the intensity of light reflected from corroded surfaces as a function of the angle of incidence, was used to detect changes on the surface of the samples. The value of the results obtained in this part of the investigation is, however, not clear. It is also stated that definite indications were found that the presence of HF in the UF_6 substantially increased the corrosion rate. The final conclusion was that the excellent properties of nickel, copper and aluminium had been proved, and that ordinary steels performed highly satisfactorily. The corrosion resistance of titanium alloys was considered good and that of "stainless steels" (unspecified) with a high nickel content excellent. The addition of chromium tended to decrease corrosion resistance.

Langlois [3] conducted a laboratory study on the effect of temperature on the corrosion by UF_6 of electrically heated wires at temperatures up to 1000 °C. This technique made it possible to determine the corrosion rate continuously by measuring the change in electrical resistance of the wire as a function of time and temperature. The technique allowed corrosion studies in glass apparatus, as the UF_6 was kept at room temperature. The results are shown in figure 2.1. Nickel behaved anomalously, in the temperature range 550 to 700 °C where corrosion rates increase sharply above 550 °C, reach a maximum at about 640 °C, and then decrease to about 700 °C. The rates again increase rapidly above 800 °C. It would appear that a measure of protection is afforded by a nickel fluoride film when

---

3) G. Langlois, "Corrosion of Metallic Materials by Uranium Hexafluoride at High Temperatures," USAEC Report A.E.C.-tr-6504 translated from CEA-2385 (1963)

it is thin enough to accommodate epitaxial stresses. Above 750 °C, however, the vapour pressure of nickel fluoride becomes sufficient for it to sublime, and hence the increased corrosion rate above this temperature. These effects had been reported earlier by Hale et al.[4] when they studied pre-fluorinated nickel in UF_6 at elevated temperatures.

In figure 2.1 two curves for Monel are reported. It would seem that an effect analogous to passivation is found when the Monel is pre-treated with UF_6 at 550 - 580 °C. Under these circumstances, Monel corrodes parabolically at higher temperatures (up to 800 °C). This indicates a diffusion-controlled reaction mechanism. In view of the volatility of nickel fluoride above 750 °C, and of the sublimation of CuF_2, especially above 400 °C, as reported by Gillardeau et al.[5], this behaviour is difficult to explain. Steindler and Vogel [6] observed the violent detachment of corrosion films from Monel coupons previously exposed to fluorine at 750 °C. Exposure of the corrosion film of copper fluoride and nickel fluoride to laboratory air may have resulted in reaction of the copper fluoride with moisture with subsequent changes in density and structure. Crabtree et al.[7] studied the corrosion film formed by fluorine on copper. The fluorination temperatures ranged from 100 °C to 500 °C. The best diffraction patterns were obtained in the region of 300 °C. When a

---

4) C.F. Hale, E.J. Barber, H.A. Bernhardt and K.E. Rapp, "High temperature Corrosion Study Interim report for the period November 1958 through May 1959," AECD, 4292 (1959)

5) J. Gillardeau, Y. Macheteau, P. Plurien and J. Oudar, "Some Aspects of the Fluoridation of Copper and Iron," Oxidation of Metals 2, 319-330 (1970)

6) M.J. Steindler and R.C. Vogel, "Corrosion of Materials in the Presence of Fluorine at Elevated Temperature", ANL-5662 (1957).

7) J.M. Crabtree, C.S. Lees and F. Little, "The Copper Fluorides, Part I X-ray and Electron microscope Examination," J. Inorganic and Nuclear Chemistry, 1, 213-217 (1955)

diffraction pattern was obtained within 2 minutes of exposure to fluorine, only the diffraction lines of anhydrous cupric fluoride were present. On standing the sample in air, the corrosion film was converted to the green basic fluoride.

Dixmier et al.[8,9] described how the special properties of uranium hexafluoride influenced their choice of experimental methods. Both continuous and discontinuous measurements were made and corrosion product analysis was carried out by means of X-ray diffraction and electron diffraction. The corrosion products were found to consist mainly of fluorides of the corroding metal as well as intermediate uranium fluorides as predicted by the Agron diagram. Under some conditions the corrosion products were non-adherent or disintegrated on contact with air. Special precautions were therefore required in order to obtain accurate results. It sometimes required removal of reaction products from specimens and evaluation of mass losses. It was assumed that the mass loss method could be applied only when the metal removed by dissolution constituted less than 10 % of the weight loss due to corrosion.

Weighing did not always reflect the true corrosion behaviour of the metals studied, as the corrosion process frequently manifested itself in micro pitting. A special technique based on controlled

---

8) J. Dixmier, R. Hasson, S. Maraval and L.M. Vincent, J. Nucl. Mat. 3, 41-59 (1961)

9) J. Dixmier, R. Hasson, S. Maraval and L.M. Vincent, J. Nucl. Mat. 5, 200-207 (1961)

polishing was developed to study the depth of pitting.

In the second part of the review [9], the causes for poor reproducibility generally experienced in UF_6 corrosion studies were analysed. The main sources of error were found to be : differences in surface preparation, weighing errors, temperature variations, heterogeneity of test materials and uncertainties in UF_6 pressure.

Vincent, Dixmier and Hasson [10] described some of the corrosion processes occurring on different metals. In the temperature range 150 to 200 ^{o}C they found clearly defined corrosion layers. Iron displayed a primary film in close contact with the metal surface followed by a layer of FeF_3 and a layer of intermediate uranium fluorides. It was found that the Agron diagram did not always accurately predict the nature of the intermediate fluorides. At lower temperatures the same constituents were found, although the layers appeared to be much more complex. Evidence was found for the existence of UF_6-metal complexes. These complexes were thought to be thermally unstable and therefore did not exist above say, 120 ^{o}C. At temperatures above 400 ^{o}C only metal fluorides could be detected on the surface. These fluoride layers were sometimes non-adherent or powdery, as in the case of iron. Several metallurgical factors and their influence on corrosion by UF_6 are discussed. These will be briefly reviewed:

---

10) L.M. Vincent, J. Dixmier and R. Hasson, Industries Atomiques 1/2, 67 (1963)

It was found that impurities not in solid solution frequently act as nuclei for growths consisting of intermediate uranium fluorides. Some precipitates are attacked selectively :

In steels	: sulphides, oxides, silicates.
In stainless steels	: carbides, sulphides, manganese silicates, carbo-nitrides of titanium, oxides.
In light metals	: Mg_2Si and Al_3Fe.
In copper	: Cu_2O and Cu-Cu_2O eutectic.
In Monel	: carbo-nitrides of titanium, sulphides and oxides of magnesium.

In leaded bronze, the presence of lead leads to much higher corrosion rates. Selective attack on grain boundaries due to segregation (e.g. Fe-Cr intermetallic compounds) occurs generally. Carbides in ferritic stainless steel were also found to be preferentially attacked.

In materials containing graphite, disintegration of the specimen normally occurs. Cast irons are attacked vigorously. The behaviour of steels is strongly dependent on the carbon content, as shown in figure 2.2.

It was found that metallographic polishing with alumina or diamond paste lowered corrosion rates by a factor of three compared to machined surfaces. Electrolytic polishing lowered rates by a factor of ten compared to mechanically polished surfaces. Surface oxides influenced the rate of attack.

Regarding factors external to the metal, the authors stressed the necessity of employing pure UF_6. The presence of HF proved particularly harmful. It was found that the pressure of UF_6 had little influence on the corrosion processes, especially at the lower temperatures.

The behaviour of iron of commercial purity is discussed by Dixmier et al.[11] They made use of various techniques, including micro-weighing, micrographic analysis and chemical analysis. At temperatures above 300 ^{o}C corrosion was followed by studying the increase in electrical resistance of a wire heated by the Joule effect. The direct observation of the initial stages of corrosion was made possible through the use of a specially developed hot stage (described in a separate publication).[12] Typical corrosion isotherms found for steel C10c are shown in figure 2.3.

In the region 50 - 100 ^{o}C a corrosion activiation energy of 21 kJ mol^{-1} was found. This increased to 29 kJ mol^{-1} in the range 100 - 200 ^{o}C.

Examination of the metal, stripped from its corrosion products, showed that at 80 ^{o}C essentially micropitting of ferrite grains occurred. At the same time inclusions, particularly manganese sulphide, were vigorously attacked. At somewhat higher temperatures (100 - 120 ^{o}C) grain boundaries were etched. Tertiary cementites and oxides were attacked. In the region of 150 - 200 ^{o}C attack on the grains was pronounced.

---

11) J. Dixmier, L.M. Vincent and R. Hasson, Corrosion et Anticorrosion, 11, 86-97 (1963)

12) L.M. Vincent and R. Hasson, Mémoires Scientifiques Rev. Métallurg, LXII, No. 5, 414-419 (1965).

At low temperatures (60 - 100 ^{o}C), interference colours could be observed as the metal surface was brought into contact with UF_6. The reaction rate strongly depended on crystal orientation because different crystals developed different colours. Manganese sulphide rapidly changed colour and became surrounded by a crown of micro-crystals. The growth process of the base film was followed microscopically. It was initiated by the appearance of "steps", as shown in figure 2.4. Lateral extensions of these steps tended to fill the gaps between them, while secondary "steps" appeared on the new surfaces thus created.

Above 100 ^{o}C the attack of new inclusions became apparent such as tertiary cementites and oxides. When 150 ^{o}C was reached, the growth of subfluorides became active and rapid and the surface appeared entirely covered with a deposit which upon micrographic examination resolved into a close mass of crystallites.

At 200 ^{o}C the samples were covered in a dense thick crust in which internal stresses caused scaling, continuously exposing new surface and therefore leading to linear kinetics in this temperature region. Under the surface layer a second layer, green in colour, could be observed.

Analysis of products formed in the 80 - 100 ^{o}C region indicated a uranium subfluoride content of more than 90 %. This was thought to be mainly UF_5.

The black outer layer formed at 250 ^{o}C was found to be U_2F_9, as predicted by the equilibrium diagram. The subjacent green layer was identified as FeF_3. The sublayer which adhered more or

At low temperatures (60 - 100 ^{o}C), interference colours could be observed as the metal surface was brought into contact with UF_6. The reaction rate strongly depended on crystal orientation because different crystals developed different colours. Manganese sulphide rapidly changed colour and became surrounded by a crown of micro-crystals. The growth process of the base film was followed microscopically. It was initiated by the appearance of "steps", as shown in figure 2.4. Lateral extensions of these steps tended to fill the gaps between them, while secondary "steps" appeared on the new surfaces thus created.

Above 100 ^{o}C the attack of new inclusions became apparent such as tertiary cementites and oxides. When 150 ^{o}C was reached, the growth of sub-fluorides became active and rapid and the surface appeared entirely covered with a deposit which upon micrographic examination resolved into a close mass of crystallites.

At 200 ^{o}C the samples were covered in a dense thick crust in which internal stresses caused scaling, continuously exposing new surface and therefore leading to linear kinetics in this temperature region. Under the surface layer a second layer, green in colour, could be observed.

Analysis of products formed in the 80 - 100 ^{o}C region indicated a uranium subfluoride content of more than 90 %. This was thought to be mainly UF_5.

The black outer layer formed at 250 ^{o}C was found to be U_2F_9, as predicted by the equilibrium diagram. The subjacent green layer was identified as FeF_3. The sublayer which adhered more or

less to the metal could not be positively identified, but was found to contain fluorine, iron and uranium.

Vincent [13] drew a parallel between dry oxidation and fluorination by certain fluorinating gases (fluorine, hydrogen fluoride, chlorine trifluoride and uranium hexafluoride). He stated that UF_6 constitutes the most complex case in view of the fact that solid uranium subfluorides are formed simultaneously with the metal fluoride at the gas-metal interface. These subfluorides are themselves liable to react with gaseous UF_6 to form a more oxidised subfluoride of uranium. Vincent concluded that fluorination reactions constitute a special case of dry oxidation by virtue of numerous parallels e.g. standard heats of formation of oxides and fluorides of a variety of metals.

Hasson and Vincent [14] studied the role of inclusions in iron, copper, nickel, lead and their alloys in corrosion by a variety of fluorinating gases (F_2, HF, $C\ell F_3$, UF_6). Generally solid deposits formed more readily on inclusions than on the matrix itself. In mild steel at low temperatures crystalline formations 20 µm thick were found on inclusions while the matrix showed only interference colours, indicating a film thickness of less than 0,5 µm. It is clear that kinetic studies relying on mass increases will lead

---

13) L.M. Vincent, Chimie Industrie - Génie Chimique 95, 611-621 (1966)

14) R. Hasson and L.M. Vincent, Mémoires Scientifiques Rev. Métallurg, LXIV, No. 3, 213-224 (1967)

to serious errors. The rôle of the inclusions can be visualized as discontinuities in the protective fluoride film leading to local attack.

Dixmier et al.[15] gave a general overview of the corrosion studies that had been undertaken by the "Group for Corrosion and Fluorination of Metals" at Saclay. The following conclusions were drawn :

> "Significant results, on which long term forecasts can be based, can only be obtained if refined methods and thorough precautions are applied.
>
> A detailed systematic study of every material is indispensable to decide on the possibilites of employ thereof. Wrong interpretation of certain factors can lead to disastrous industrial results.
>
> Extensive comprehension of the corrosion mechanisms, based on a fundamental type of research work, is indispensable if one wants to try and improve the performance of existing materials or create new materials, particularly if the lastmentioned have to comply with strict economic imperatives."

Vincent et al.[16] reviewed much of the French work up to 1969. UF_6, ClF_3 and fluorine were discussed. Experimental methods[17] were also treated in some detail.

---

15) J. Dixmier, R. Hasson, S. Maraval, P. Salle and L. Vincent, "La Corrosion des Materiaux Metalliques Dans le Procede de Diffusion Gazeuse" in "Problemi della Separazione Isotopica Dell' Uranio" pp. 199-209 (Symposium, Turin, 1-2 October 1968)

16) L. Vincent, J. Gillardeau, R. Hasson and S. Maraval, Energie Nucléaire, 11, 400-410 (1969)

17) L. Vincent, J. Gillardeau, R. Hasson and S. Maraval, Energie Nucléaire, 11, 411-422 (1969)

to serious errors. The rôle of the inclusions can be visualized as discontinuities in the protective fluoride film leading to local attack.

Dixmier et al.[15] gave a general overview of the corrosion studies that had been undertaken by the "Group for Corrosion and Fluorination of Metals" at Saclay. The following conclusions were drawn :

> "Significant results, on which long term forecasts can be based, can only be obtained if refined methods and thorough precautions are applied.
>
> A detailed systematic study of every material is indispensable to decide on the possibilites of employ thereof. Wrong interpretation of certain factors can lead to disastrous industrial results.
>
> Extensive comprehension of the corrosion mechanisms, based on a fundamental type of research work, is indispensable if one wants to try and improve the performance of existing materials or create new materials, particularly if the lastmentioned have to comply with strict economic imperatives."

Vincent et al.[16] reviewed much of the French work up to 1969. UF_6, ClF_3 and fluorine were discussed. Experimental methods[17] were also treated in some detail.

---

15) J. Dixmier, R. Hasson, S. Maraval, P. Salle and L. Vincent, "La Corrosion des Materiaux Metalliques Dans le Procede de Diffusion Gazeuse" in "Problemi della Separazione Isotopica Dell' Uranio" pp. 199-209 (Symposium, Turin, 1-2 October 1968)

16) L. Vincent, J. Gillardeau, R. Hasson and S. Maraval, Energie Nucléaire, 11, 400-410 (1969)

17) L. Vincent, J. Gillardeau, R. Hasson and S. Maraval, Energie Nucléaire, 11, 411-422 (1969)

An interesting method of enhancing the resistance of brazed aluminium alloys to corrosion by fluorinating gases is described in a United States Patent.[18] When aluminium-silicon alloy filler metal is used, brazed joints are attacked by fluorinating gases due to the formation of gaseous SiF_4. When a continuous silicon-rich phase is present in the alloy, the leaching process is continued through the joint. However, if discrete silicon-rich particles are created by suitable heat treatment the corrosion resistance of the joint is improved considerably.

---

18) D.S. McGlasson, J.T. Tidwell, C.E. Weaver and C.A. Culpepper, U.S. Patent 3 859 145 (Jan. 7,1975)

TABLE 2.1 : CORROSION RATES OF ALLOYS IN GASEOUS UF_6 AT 240 kPa AND 80 °C 2)

Alloy	Exposure Time h	Corrosion Rate µm/h x10^6
High-purity aluminium	672	58
5051 aluminium	672	116
5057 aluminium	672	87
0,12 C steel	1440	145
0,25 C steel	1440	145
0,35 C steel	1440	145
0,50 C steel	1440	145
0,65 C steel	1440	145
1,25 C steel	1440	522
Copper	720	29
Cu 30 Zn 2,5 Aℓ 1,5 Fe < 2 Ni 0,8 Si 0,8 Pb	1440	406
Cu 35 Zn 3 Pb 0,5 Fe	1440	116
Cu 11 Aℓ 6 Ni 6 Fe < 2,5 Mn	1440	58
Cu 11,5 Aℓ 4,5 Ni 4 Fe	1440	58
Monel	1440	3
Ti 6 Aℓ 4 V	504	406
Ti 5 Aℓ 2,5 Sn	504	406
Ti 8 Mn	408	493

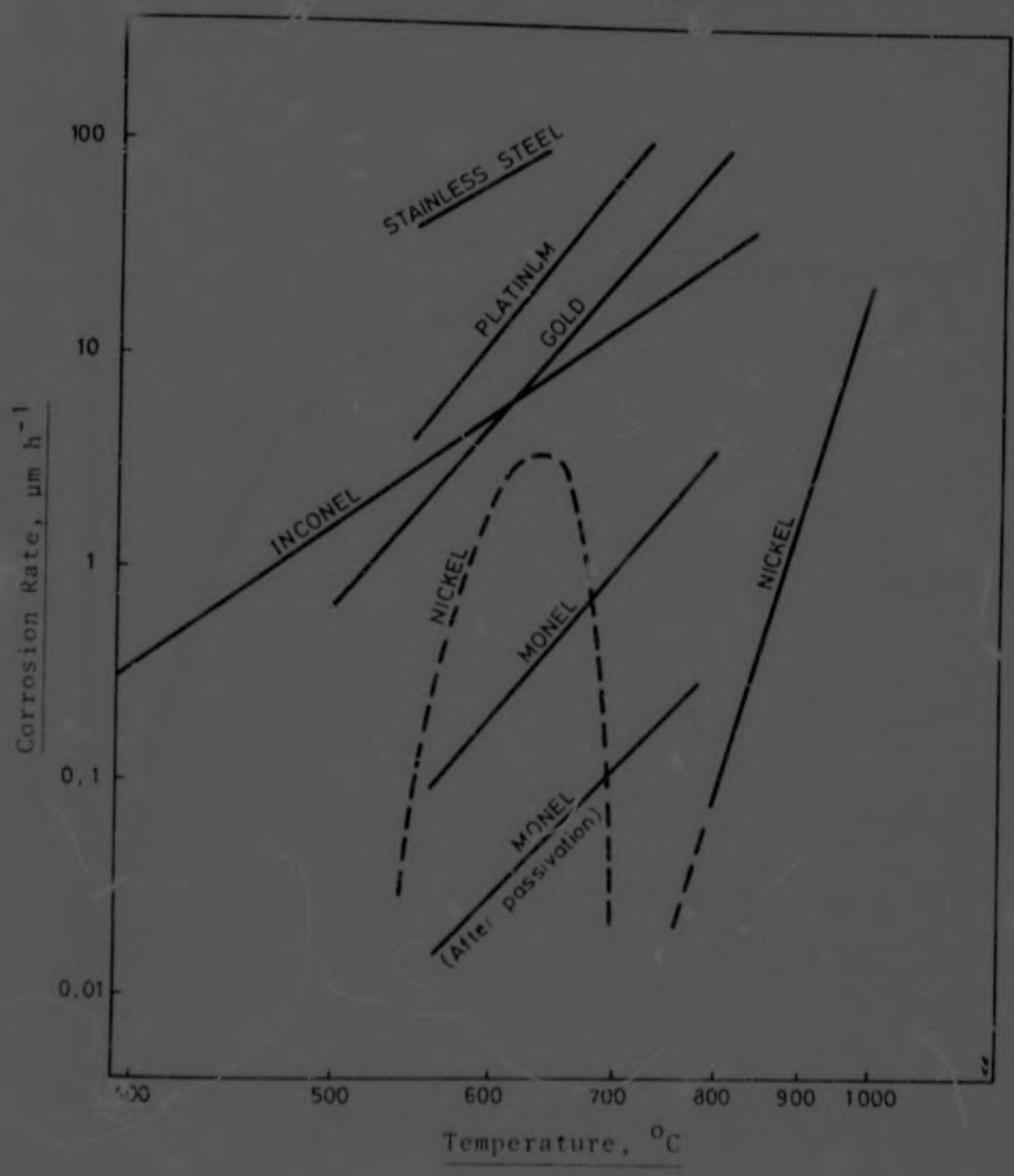

FIGURE 2.1 [3] : CORROSION RATES BETWEEN 400 °C AND 1000 °C UNDER A UF_6 PRESSURE OF 32 kPa

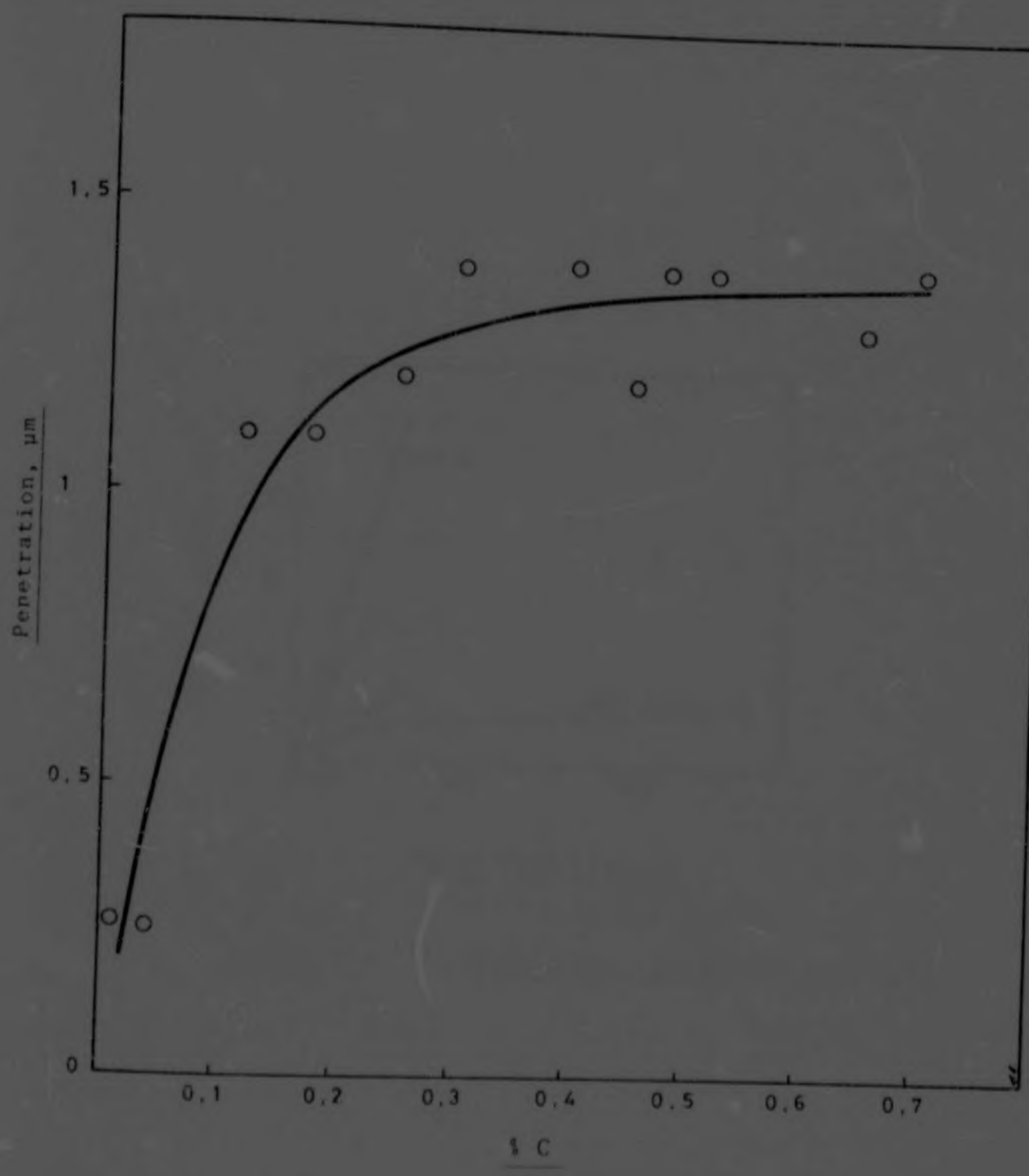

FIGURE 2.2 [10] : INFLUENCE OF CARBON ON THE PENETRATION OF STEELS EXPOSED TO UF_6 FOR 1000 h AT 100 °C

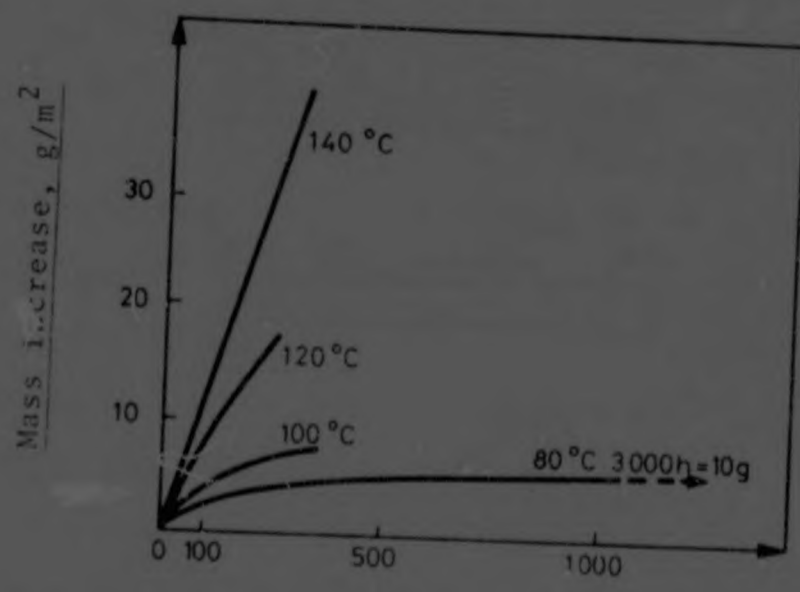

FIGURE 2.3 [11]: STEEL C10c : CORROSION ISOTHERMS

FIGURE 2.4 [11] : STEEL C10c : GROWTH OF THE INTERFERENCE FILM

3. EXPERIMENTAL PROCEDURE

3.1 Introduction

The literature survey presented in the previous chapter revealed the relative dearth of UF_6 corrosion data for many engineering materials.

As was indicated earlier, there are several reasons why all forms of corrosion must be eliminated as far as practically possible. Choice of constructional materials therefore has to be done with extreme care. As in many engineering situations, the final choice is frequently a compromise between several conflicting requirements. From a corrosion point of view, aluminium alloys constitute a very attractive class of materials for the construction of pipes, vessels etc. Factors such as economic considerations, strength requirements, manufacturing techniques etc., frequently force the hand of the metallurgist to make concessions. This leads to the use of materials such as stainless steels which have many attractive properties, although frequently considered for applications for which they were not originally designed.

Copper alloys are very useful for applications in, for instance, valves, instruments, bearings, seals, etc. Monel metal is one of the most resistant materials to fluorinating atmospheres, even at high temperatures. Copper-zinc alloys are applicable as brazing alloys and in applications where good machinability is required. Aluminium bronzes and beryllium copper are frequently employed in valves and in diaphragms respectively.

3. EXPERIMENTAL PROCEDURE

3.1 Introduction

The literature survey presented in the previous chapter revealed the relative dearth of UF_6 corrosion data for many engineering materials.

As was indicated earlier, there are several reasons why all forms of corrosion must be eliminated as far as practically possible. Choice of constructional materials therefore has to be done with extreme care. As in many engineering situations, the final choice is frequently a compromise between several conflicting requirements. From a corrosion point of view, aluminium alloys constitute a very attractive class of materials for the construction of pipes, vessels etc. Factors such as economic considerations, strength requirements, manufacturing techniques etc., frequently force the hand of the metallurgist to make concessions. This leads to the use of materials such as stainless steels which have many attractive properties, although frequently considered for applications for which they were not originally designed.

Copper alloys are very useful for applications in, for instance, valves, instruments, bearings, seals, etc. Monel metal is one of the most resistant materials to fluorinating atmospheres, even at high temperatures. Copper-zinc alloys are applicable as brazing alloys and in applications where good machinability is required. Aluminium bronzes and beryllium copper are frequently employed in valves and in diaphragms respectively.

As a result of the potentially wide applicability of copper alloys in an enrichment plant, it was decided to embark on a corrosion programme aimed at acquiring a better understanding of the corrosion behaviour of copper alloys in gaseous UF_6.

3.2 Alloys Investigated

Table 3.1 contains a list of the copper alloys studied. In most instances the alloys were specially prepared for this investigation as commercial alloys frequently contain small amounts of impurities which could influence results.

Alloys were melted in a vacuum furnace and cast into small ingots which were hot rolled down to a thickness of 1 mm. Intermediate annealing was done when required. Final annealing was normally carried out at 750 ^{o}C for 30 minutes in sealed quartz tubes under argon to prevent oxidation and excessive changes in composition such as through zinc loss in brasses.

From the 1 mm thick strips, specimens (15 mm in diameter) were punched. Brittle alloys were used in the as-cast condition, specimens being machined to the required dimensions.

Chemical analysis was carried out on all alloys using wet chemical methods, spectrography and atomic absorption spectroscopy.

3.2.1 Aluminium bronze

Aluminium bronzes are a group of copper alloys containing aluminium as the principal alloying element which are renowned for their high strength and excellent corrosion resistance. Aluminium bronzes are equally suitable for casting and mechanical working. With less than about 8 per cent of aluminium the alloys have an essentially ductile structure. Addition of iron gives rise to an improvement in both strength and corrosion resistance. Typical applications of cast and wrought aluminium bronze include impellers, bearings, gears, heat exchangers, pressure vessels, compressor blades etc. The alloy included in this investigation was supplied by McKechnie Bros.

As a result of the potentially wide applicability of copper alloys in an enrichment plant, it was decided to embark on a corrosion programme aimed at acquiring a better understanding of the corrosion behaviour of copper alloys in gaseous UF_6.

3.2 Alloys Investigated

Table 3.1 contains a list of the copper alloys studied. In most instances the alloys were specially prepared for this investigation as commercial alloys frequently contain small amounts of impurities which could influence results.

Alloys were melted in a vacuum furnace and cast into small ingots which were hot rolled down to a thickness of 1 mm. Intermediate annealing was done when required. Final annealing was normally carried out at 750 ^{o}C for 30 minutes in sealed quartz tubes under argon to prevent oxidation and excessive changes in composition such as through zinc loss in brasses.

From the 1 mm thick strips, specimens (15 mm in diameter) were punched. Brittle alloys were used in the as-cast condition, specimens being machined to the required dimensions.

Chemical analysis was carried out on all alloys using wet chemical methods, spectrography and atomic absorption spectroscopy.

3.2.1 Aluminium bronze

Aluminium bronzes are a group of copper alloys containing aluminium as the principal alloying element which are renowned for their high strength and excellent corrosion resistance. Aluminium bronzes are equally suitable for casting and mechanical working. With less than about 8 per cent of aluminium the alloys have an essentially ductile structure. Addition of iron gives rise to an improvement in both strength and corrosion resistance. Typical applications of cast and wrought aluminium bronze include impellers, bearings, gears, heat exchangers, pressure vessels, compressor blades etc. The alloy included in this investigation was supplied by McKechnie Bros.

3.2.2 Copper-zinc alloys

This system was investigated more intensively than the others. The alloys investigated are indicated on the phase diagram[1] (figure 3.1), from which it can be seen that alloys consisting of the α, $\alpha + \beta'$, β', $\gamma + \varepsilon$ and $\varepsilon + \eta$ phases were studied.

Three commercial alloys (supplier: McKechnie Bros.) were included, namely Cu 10 Zn, Cu 30 Zn and a leaded brass - Cu 29 Zn 1 Pb.

From an industrial viewpoint, the α- and $\alpha\beta$-brasses probably form the most important series of copper alloys. The higher zinc content alloys were, however, included in this project with a view to gaining a complete picture of the copper-zinc system.

Lead is normally added to enhance the casting properties and machinability, and appears in the microstructure as small interdendritic globules.

Selected micrographs of the alloys studied are presented in figures 3.2 to 3.6.

3.2.3 Copper-zinc-tin alloys

Both admiralty brass (70 Cu 29,5 Zn 0,5 Sn) and Naval brass (60 Cu 39 Zn 1 Sn) were included in this study.

Tin is normally added to resist dezincification in these alloys when used in marine environments, and is also thought to influence resistance to stress corrosion cracking.

---

[1] C.J. Smithells, "Metals Reference Book", Volume II, Butterworths (1967).

Naval brass is well known for its hot working properties, ascribed to the presence of the β phase which is easily deformed at elevated temperatures.

The microstructures of these two alloys are shown in figures 3.7 and 3.8.

3.2.4 Copper-tin alloys

The copper-tin phase diagram is shown in figure 3.9.[1] The diagram indicates that both alloys studied, 95 Cu 5 Sn and 90 Cu 10 Sn, consist of α + ε solid solution at equilibrium. Phosphorus is added to deoxidize the metal, but the concentration rarely exceeds 0,04 %, and the element is not detectable in the microstructure. Equilibrium is not easily reached even at 600 °C. The microstructure therefore, consists of the α phase only in the form of equi-axed grains exhibiting twins. (See figure 3.10.)

These alloys find application in the work-hardened condition in instrument parts, springs of all types and as bearings.

3.2.5 Beryllium copper

This material presents an interesting example of an alloy susceptible to precipitation hardening, as is revealed by the phase diagram (figure 3.12)[2]. The microstructure (figure 3.13) contains small spherical particles of β in a fine-grained α matrix as a result of incomplete suppression of the former constituent during cooling from elevated temperatures. The alloy studied contained 0,27 % Co which is added to control the rate of precipitation. Some of the cobalt appears in the microstructure as relatively

---

2) "Copper and Copper Alloys - Selected Microstructures and Equilibrium Diagrams". C.D.A. Publication No. 64. (1962).

large particles of CoBe which are pale blue in colour.

The alloy studied was in the ½ H condition (solution treated, quenched in water, 20 % cold rolled) and had a hardness of R_B 92. These alloys are well-known spring materials and are used in bellows and in pressure-responsive devices.

3.2.6 Nickel silver

Copper alloys containing nickel and zinc as alloying elements are known as "nickel silvers" on account of their colour. The alloy studied (55 Cu 27 Zn 18 Ni) shows a typical structure consisting of the α phase in equi-axed grains exhibiting twins. (See figure 3.14.)

The α alloys are industrially the most important nickel silvers. They have good ductility and strength and are readily cold worked into rolled products, wire etc.

3.3 Specimen preparation

At the outset it was realized that, owing to the sensitivity of UF_6 to the condition of the surface, sample preparation constituted the most critical phase of the investigation.

As chemical cleaning is invariably applied to all process equipment before UF_6 contact, and as this normally entails some form of chemical polishing or light etching, it was decided to subject all samples to brief electropolishing before initial weighing.

All the alloys, excepting phosphor bronze, polished satisfactorily in an electrolyte containing 408 g dm^{-3} H_3PO_4. Phosphor bronze was polished in a mixture consisting of 1 150 g dm^{-3} H_3PO_4

and 172 g dm^{-3} H_2SO_4. Polishing times were kept very short (5 - 15 seconds) in view of the danger of substantially changing the surface composition and preferentially removing inclusions or certain phases.

Subsequent corrosion results, however, displayed excessive scatter. The reason for this is unknown but could relate to surface oxides and/or phosphates originating from the polishing process. These surface layers could also have accommodated relatively large amounts of bound water which on reaction with UF_6 could form solid reaction products on specimens.

The decision was therefore taken to discard the results obtained in the early part of the investigation.

After several trials it was decided to adopt the following procedure : Specimens were metallographically polished to 1 000 grit on emery paper and introduced into the corrosion apparatus. Evacuation was then carried out to a vacuum of 10^{-4} Pa, and the temperature increased to 150 ^{o}C. Pure hydrogen was introduced. Heating in hydrogen was carried out for 22 h, followed by evacuation which was maintained while the temperature was dropped to the predetermined corrosion temperature. On reaching the required temperature UF_6 was introduced. This method proved to be cumbersome but led to very low scatter in the results.

3.4 UF_6 Handling and Corrosion Testing

Various methods of corrosion testing were employed in this investigation. Gas handling equipment as well as the corrosion chambers were of all-aluminium welded construction. The

aluminium surfaces were chemically polished in a phosphoric acid/ nitric acid mixture at 80 °C, followed by water rinsing, rinsing in a dilute sodium carbonate solution, rinsing, a dilute nitric acid dip and a final rinse in demineralized water. Drying was carried out in an oven at 120 °C after swirling in chemically clean propanol.

A high standard of cleanliness was maintained throughout the investigation. Fingerprints and traces of grease or oil on specimens are particularly undesirable. Vacuum tightness of all equipment handling UF_6 is of prime importance. Ingress of traces of moist air can lead to an "aerosol" of finely divided UO_2F_2 which will settle out on specimens, leading to erroneous results. For this reason it was standard practice to leak test all equipment regularly using a helium mass spectrometer leak detector.

After specimen preparation and drying in chemically clean acetone, weighing was carried out on a microbalance, before the specimens were inserted in the corrosion chambers. Triplicate samples were exposed in separate corrosion chambers. The test temperatures were 50, 80, 100, 120 and 150 °C. Exposure times were nominally 5 h, 20 h, 50 h, 200 h and 1 000 h. As nineteen different alloys were studied, it follows that this part of the investigation entailed the processing of 1425 individual specimens.

3.4.1 Corrosion testing under constant UF_6 pressure

The corrosion apparatus for this type of investigation is shown in figure 3.15. It consists of several corrosion chambers interconnected by means of aluminium pipes. Individual chambers (figure 3.16) could be isolated by means of all-metal vacuum valves.

Samples were suspended from beryllium copper hooks fastened on to the aluminium thermocouple sheath in order to eliminate possible galvanic effects.

After insertion of the samples, vacuum was drawn through a liquid nitrogen cooled cold trap by means of an oil diffusion pump to a pressure of 10^{-4} Pa before the operations described in section 3.3 could commence.

The apparatus made provision for cooling of the UF_6 supply vessel to temperatures between ambient and 0 ^{o}C by means of a refrigeration unit. This ensured that any UF_6 pressure between 2,4 and 15,7 kPa could be maintained throughout long term exposures.

Before UF_6 was introduced into the evacuated chambers, it was necessary to remove HF, which always builds up in UF_6 containers. Figure 3.17[3)] shows that between - 80 ^{o}C and - 40 ^{o}C the large difference in the vapour pressures of UF_6 and HF provides a means for eliminating HF. UF_6 was therefore condenced by means of an ethanol-dry ice mixture at about - 50 ^{o}C and evacuation carried out through a liquid nitrogen cold trap. HF and other incondensible gases which might have been present were therefore seperated from the solid UF_6 and condenced in the liquid nitrogen trap.

Corrosion chambers were heated individually by means of small electric heaters. Temperature controllers facilitated the selection of temperatures up to 200 ^{o}C. The temperature of each individual chamber, normally containing 8 specimens, was recorded continuously by means of a strip chart recorder.

---

3) G. Langlois, "Corrosion of Metallic Materials by Uranium Hexafluoride at High Temperatures, "USAEC Report A.E.C.-tr-6504 translated from CEA-2385 (1963).

Generally, the apparatus performed satisfactorily. It was observed, however, that variations in corrosion rates did occur between identical specimens in different corrosion chambers although they were all inter-connected and connected to the UF_6 supply vessel. It is known that UF_6 gas is very viscous and that gas movement could be sluggish, especially through thin pipes. The greater part of the investigation was therefore carried out by means of isolated corrosion vessels as described below.

3.4.2 Corrosion testing in isolated corrosion chambers

Experience has shown that corrosion rates are not very sensitive to UF_6 pressure variations in the pressure range 5 - 20 kPa. In order to eliminate the problems discussed in the previous section, it was decided to use corrosion test vessels which could be charged with a definite amount of UF_6, and which could then be isolated from the UF_6-supply vessel and placed in an oven kept at the desired temperature. This method meant that a continuously decreasing pressure of UF_6 would be present, but by limiting the number of specimens it was ensured that total UF_6 consumption was less than 50 % of the initial charge.

Each corrosion chamber consisted of a 140 mm length of 50 mm 50S aluminium pipe with 1 mm aluminium discs welded to both ends. A 12 mm pipe and vacuum valve protruded from the body of the chamber to facilitate vacuum and gas handling.

This method of corrosion testing was less time-consuming and led to very accurate corrosion results.

Figure 3.18 shows a number of corrosion chambers being loaded with UF_6 before isolation from the gas handling rig.

3.4.3 Corrosion testing by monitoring loss of UF_6 ("Manometric method")

Equipment was also available whereby the UF_6 content of the corrosion chambers described in the previous section could be monitored without the need to remove samples from the chambers. Thus a complete corrosion/time curve could be established, using only one specimen.

This method proved particularly useful in "temperature-jump" experiments aimed at determining the activation energy.

3.5 Assessment of Quantitative Corrosion Results

Study of corrosion/time curves, supplemented by more qualitative observations, provides valuable information. The immediate aim was therefore to establish corrosion/time relationships for the nineteen alloys in question. This was done by fitting the average mass increases per cm^2 and appropriate exposure times to the general power law

$$\Delta m = At^n$$

(with Δm = mass increase and t = time) using a computer. Values of the rate constant A and exponent n were therefore obtained for the different corrosion temperatures. The Arrhenius type plot of rate constant vs. reciprocal of the absolute temperature yields the activation energy.

The results obtained from the "manometric" experiments were in terms of loss of UF_6 which, it was assumed, had reacted with the specimen. This assumption was proved to be basically correct as dummy corrosion chambers filled with UF_6 to the same initial pressure

retained on the average 96 % of their UF_6 after 1 000 h at 150 °C. Results obtained by this method did not differ from results obtained using weighing techniques.

3.6 Post-corrosion Examination

A variety of techniques was used to study specimens after exposure to UF_6 :

3.6.1 Optical microscopy

It was sometimes required to investigate corrosion layers in section. This constituted a problem in that the layers tended to be brittle and were therefore detached from the surface during polishing. To circumvent this problem the following procedure was adopted: After removal of specimens from the UF_6, they were gold plated in an ion sputtering coater. This was followed by a thin layer of electroless nickel plating which was subsequently built up to several millimeters of nickel by conventional electroplating. Metallographic polishing was then carried out dry until the final stages when alcohol was used as carrier for the diamond paste. In other instances, a "multiple sandwich" was prepared by stacking samples, interspersed with a quick hardening adhesive * to ensure protection.

The following etching reagent was used : Potassium dichromate : 18 g dm^{-3}; H_2SO_4 : 136 g dm^{-3}; HCℓ : 2 g dm^{-3}.

---

* Hottinger Baldwin Messtechnik G.m.b.H. Schnellklebstoff X60

3.6.2 Electron microscopy

Both transmission electron microscopy and scanning electron microscopy of corroded specimens were undertaken.

Scanning electron microscopy proved very useful for the study of corrosion crusts due to its exceptional depth of focus and high magnification. Two instruments were available. The Jeol JSM-U3 instrument was fitted with an Edax energy-dispersive X-ray analyser which facilitated X-ray fluorescence analyses of discrete points. The Hitachi-Akashi Minisem MSM-4 table top microscope proved especially valuable in this study due to ease of operation.

It was sometimes advantageous to detach corrosion films from the substrate in order to examine the metal/corrosion product interface. This was done by pressing scotch tape onto the corroded surface which on subsequent removal retained some corrosion product. As these layers were non-conducting, gold coating was generally required before S.E.M.-studies could be carried out.

3.6.3 Auger spectroscopy

Auger spectroscopy proved to be a valuable tool in the study of corrosion processes. As only elements present in a surface region of approximately 5 atomic layers are detected, observations on heavily corroded surfaces have little value, but in the present investigation penetration of surfaces by fluoride ion could be detected in sectioned specimens.

Auger electron spectroscopy has several real advantages :

(i) Light elements are readily detected. The technique is therefore complementary to X-ray fluorescence.

(ii) The method is non-destructive.

(iii) Extremely thin layers on the surface can be detected.

(iv) The method is sensitive.

3.6.4 X-ray analysis

Two techniques were employed to obtain X-ray analyses from corroded surfaces. The first technique involved the removal of corrosion specimens from the corrosion chambers in a glove box under dry argon and its introduction into a Lihl furnace which facilitated diffraction in the absence of air.

In the second method use was made of a specially constructed reaction vessel that could be fitted to the Siemens diffractometer (see figure 3.19). Two 30 µm thick aluminium windows allowed the passage of X-rays. The specimen was accurately aligned before the vessel was evacuated and back-filled with UF_6 to a pressure of 8 kPa. The vessel was then placed in a temperature-regulated oven and removed from time to time for diffraction analysis. Provision was made for a "cold finger" into which UF_6 could be frozen during a diffraction run. This was necessary to deminish the absorption of the X-rays by the gas. This technique made it possible to monitor reactions over long periods of time.

3.7 Oxidation

Following the initial experience with electropolished specimens, it was decided to investigate briefly the influence on UF_6 corrosion of thin oxide layers formed at 150 ^{o}C. Cu-Zn alloys were oxidized for 15 minutes in air after mechanical polishing.

TABLE 3.1 : ALLOYS INVESTIGATED

ALLOY	COMPOSITION (% BY MASS)	CONDITION
Electrolytic Cu	99,7 Cu	Annealed
95/5 Brass	94,8 Cu 5,2 Zn	Rolled/Annealed
90/10 Brass	90,0 Cu 10,0 Zn	Rolled/Annealed
85/15 Brass	84,5 Cu 15,5 Zn	Rolled/Annealed
80/20 Brass	79,2 Cu 20,8 Zn	Rolled/Annealed
70/30 Brass	70,9 Cu 29,1 Zn	Rolled/Annealed
70/30 Brass (Commercial alloy)	71,0 Cu 29,0 Zn	Rolled/Annealed
Muntz metal	58,5 Cu 41,5 Zn	Cast/Annealed
50 Cu 50 Zn	52,4 Cu 47,6 Zn	Cast
25 Cu 75 Zn	25,4 Cu 74,6 Zn	Cast
10 Cu 90 Zn	9,6 Cu 90,4 Zn	Cast
Admiralty Brass	70,4 Cu 29,3 Zn 0,3 Sn	Cast
Naval Brass	59,8 Cu 39,0 Zn 1,2 Sn	Cast/Annealed
Leaded Brass	66,9 Cu 32,3 Zn 0,8 Pb	Rolled
95/5 Phosphor Bronze	94,8 Cu 5,2 Sn	Rolled/Annealed
90/10 Phosphor Bronze	87,9 Cu 12,1 Sn	Cast
Beryllium Copper	97,97 Cu 1,7 Be 0,27 Co	½ H
18 % Nickel Silver	55,1 Cu 18,4 Ni 26,5 Zn	Rolled/Annealed
Aluminium Bronze	89,9 Cu 6,9 Al 2,7 Fe	Rolled

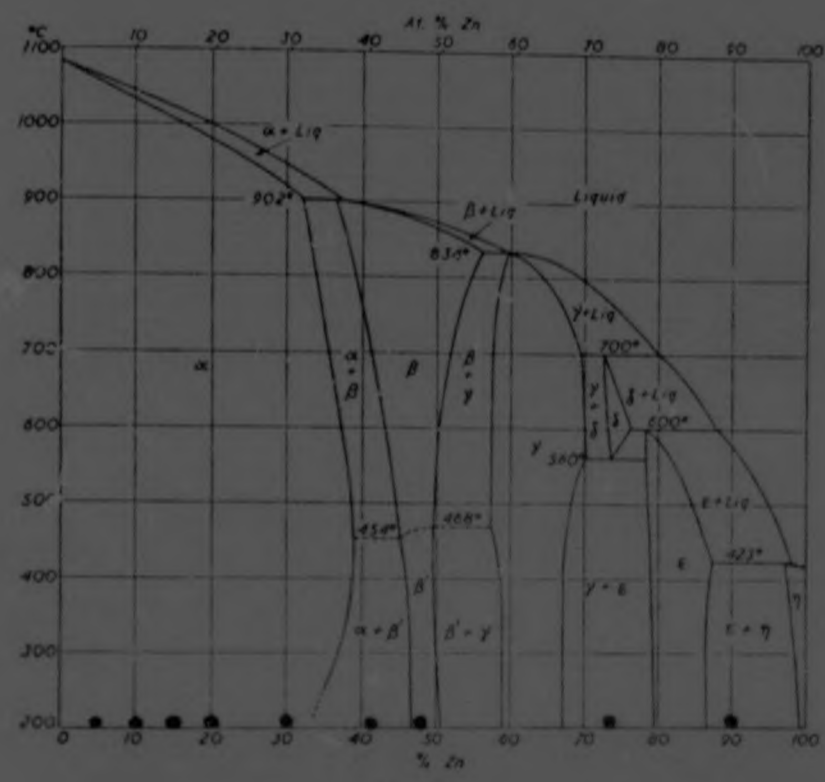

Cu-Zn

FIGURE 3.1 : COPPER-ZINC PHASE DIAGRAM

(Alloys studied are indicated)

FIGURE 3.2 : Cu 20 Zn (x 200)

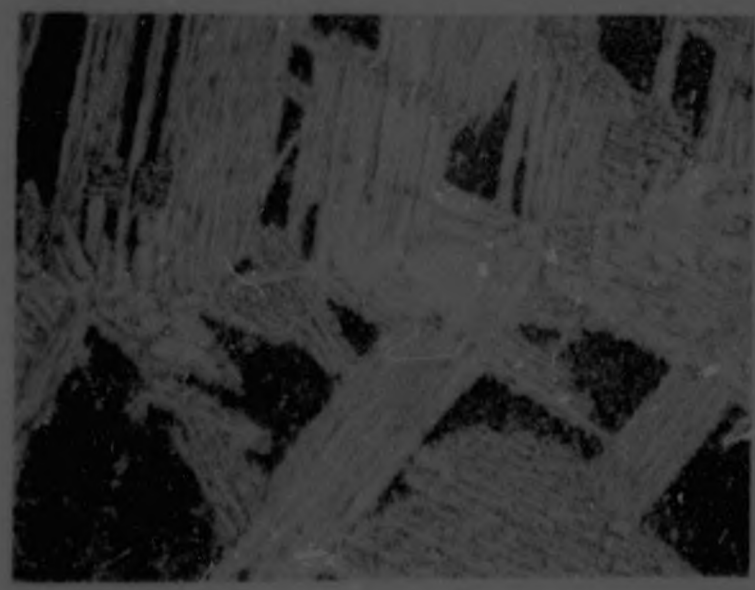

FIGURE 3.3 : Cu 40 Zn (x 400)

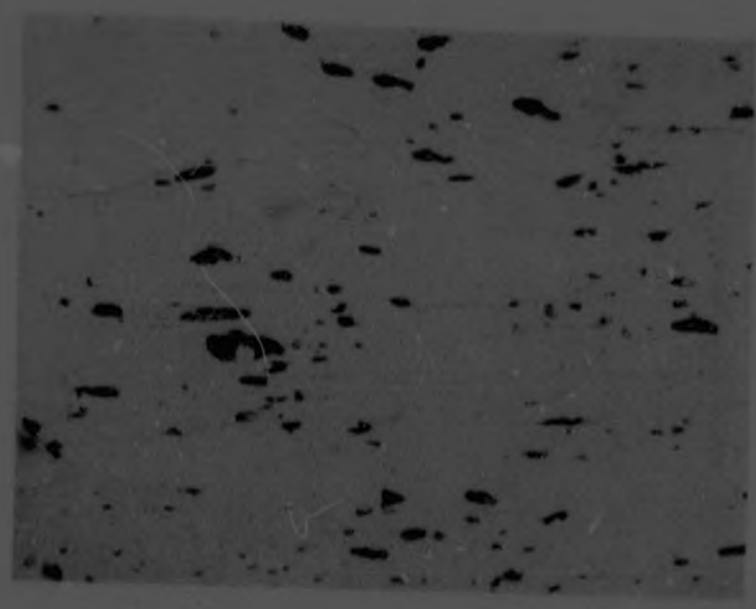

FIGURE 3.4 : LEADED BRASS (x 400)

FIGURE 3.5 : Cu 75 Zn (x 400)

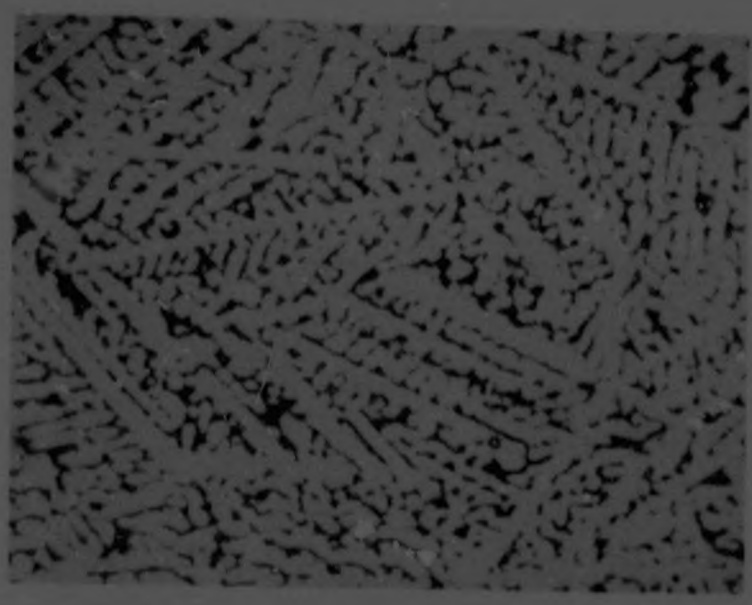

FIGURE 3.6 : Cu 90 Zn (x 400)

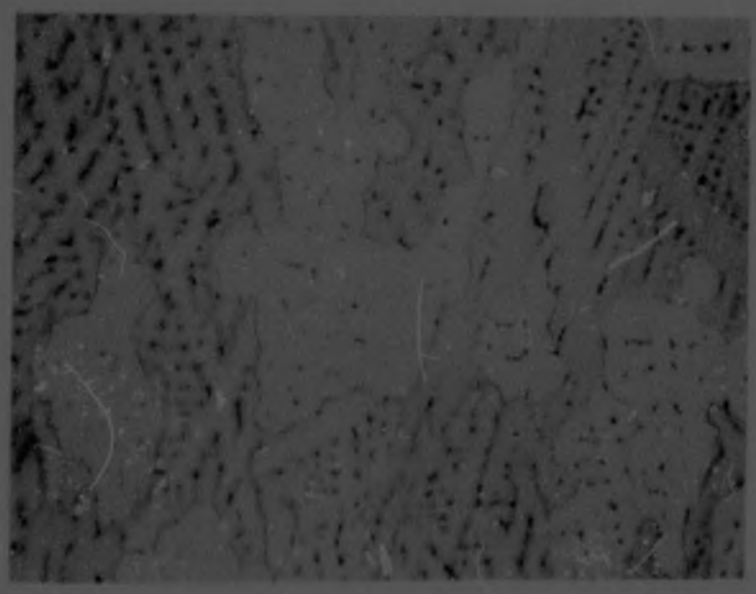

FIGURE 3.7 : ADMIRALTY BRASS (x 500)

FIGURE 3.8 : NAVAL BRASS (x 100)

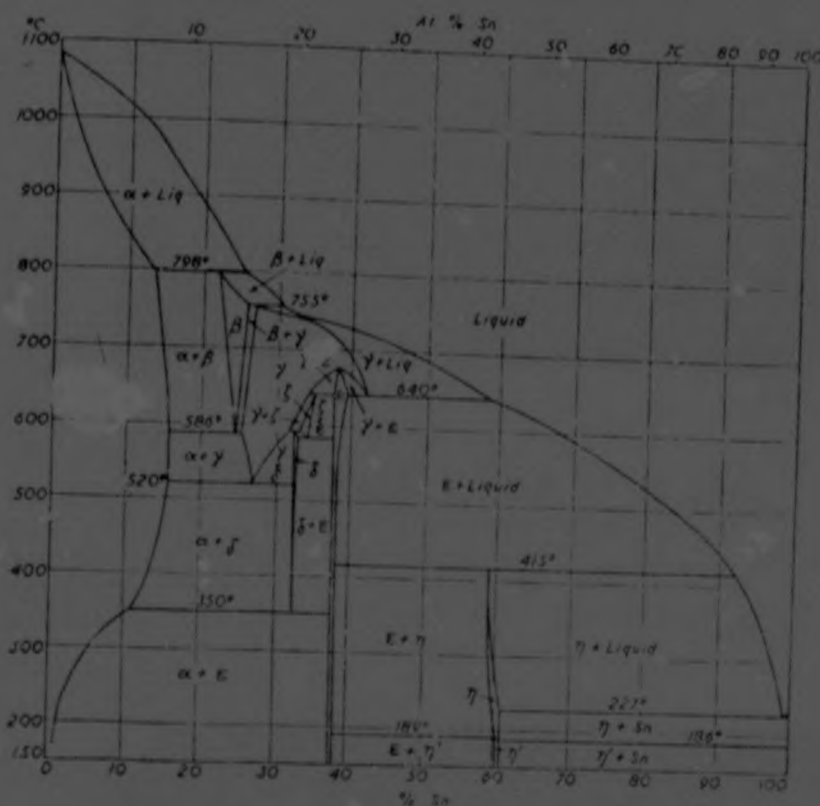

Cu-Sn

FIGURE 3.9 : COPPER-TIN PHASE DIAGRAM

FIGURE 3.10 : Cu 5 Sn (x 200)

FIGURE 3.11 : Cu 10 Sn (x 200)

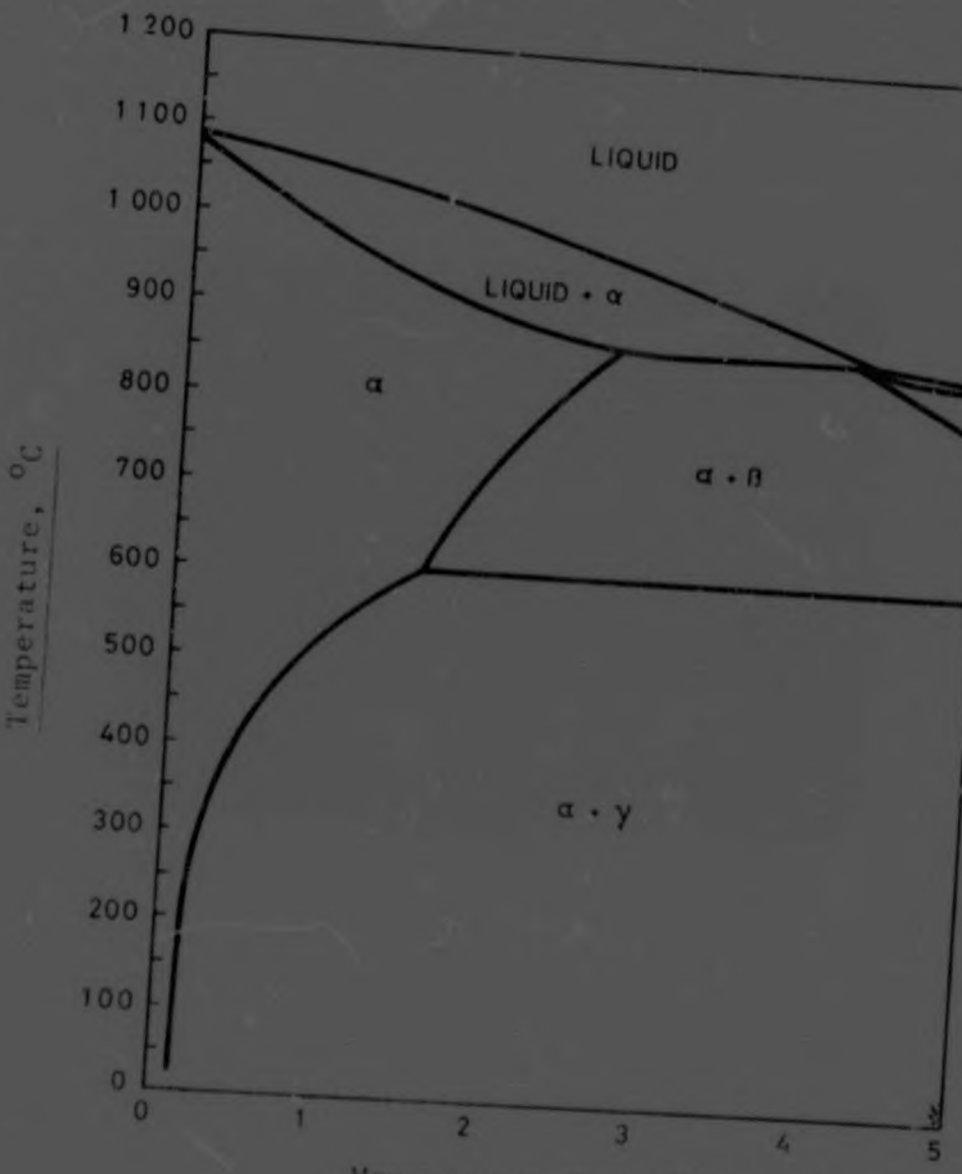

FIGURE 3.12 : COPPER-BERYLLIUM PHASE DIAGRAM

FIGURE 3.13 : BERYLLIUM COPPER (x 400)

FIGURE 3.14 : 18 % NICKEL SILVER (x 325)

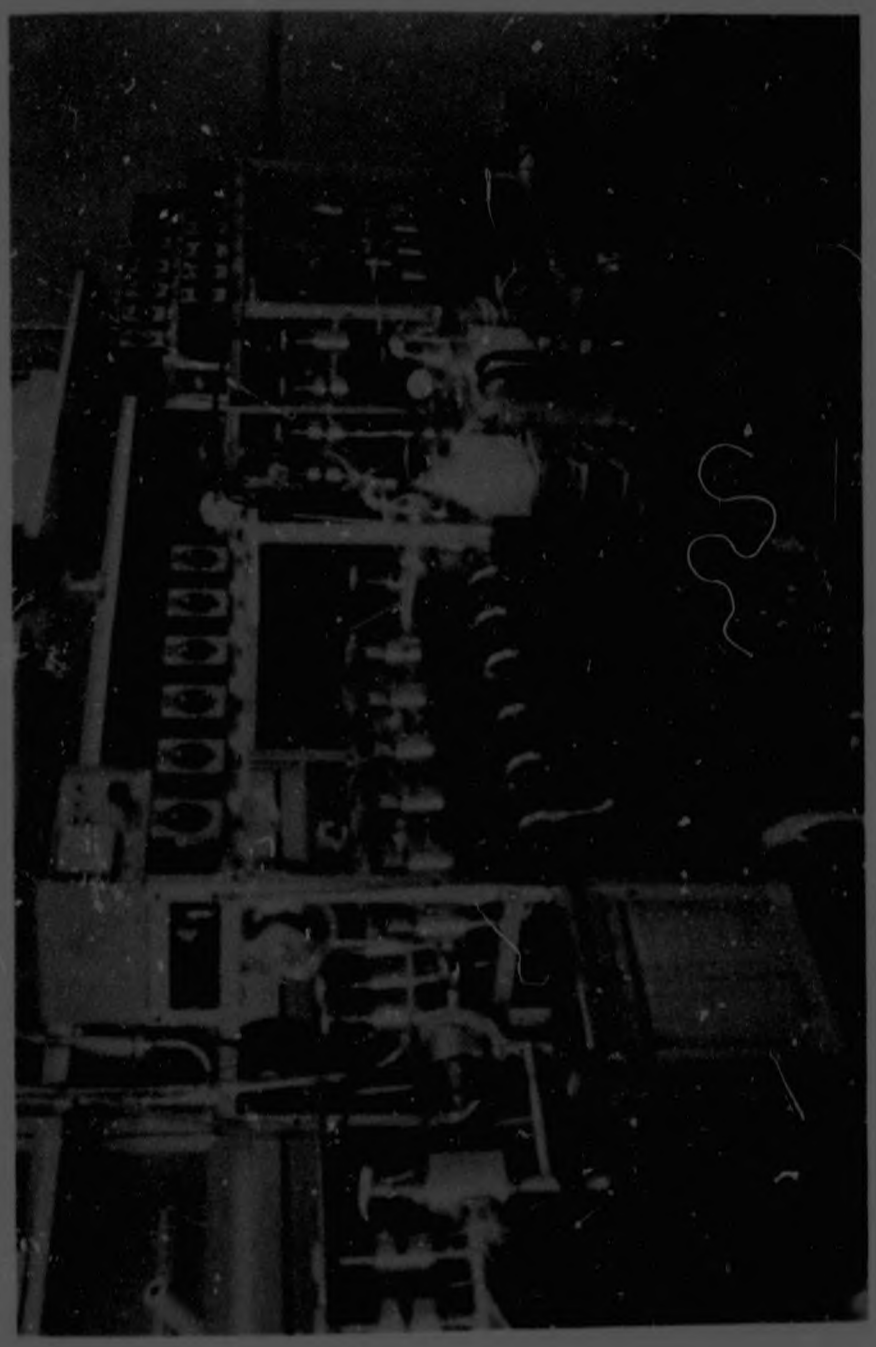

FIGURE 3.15 : UF_6 CORROSION APPARATUS

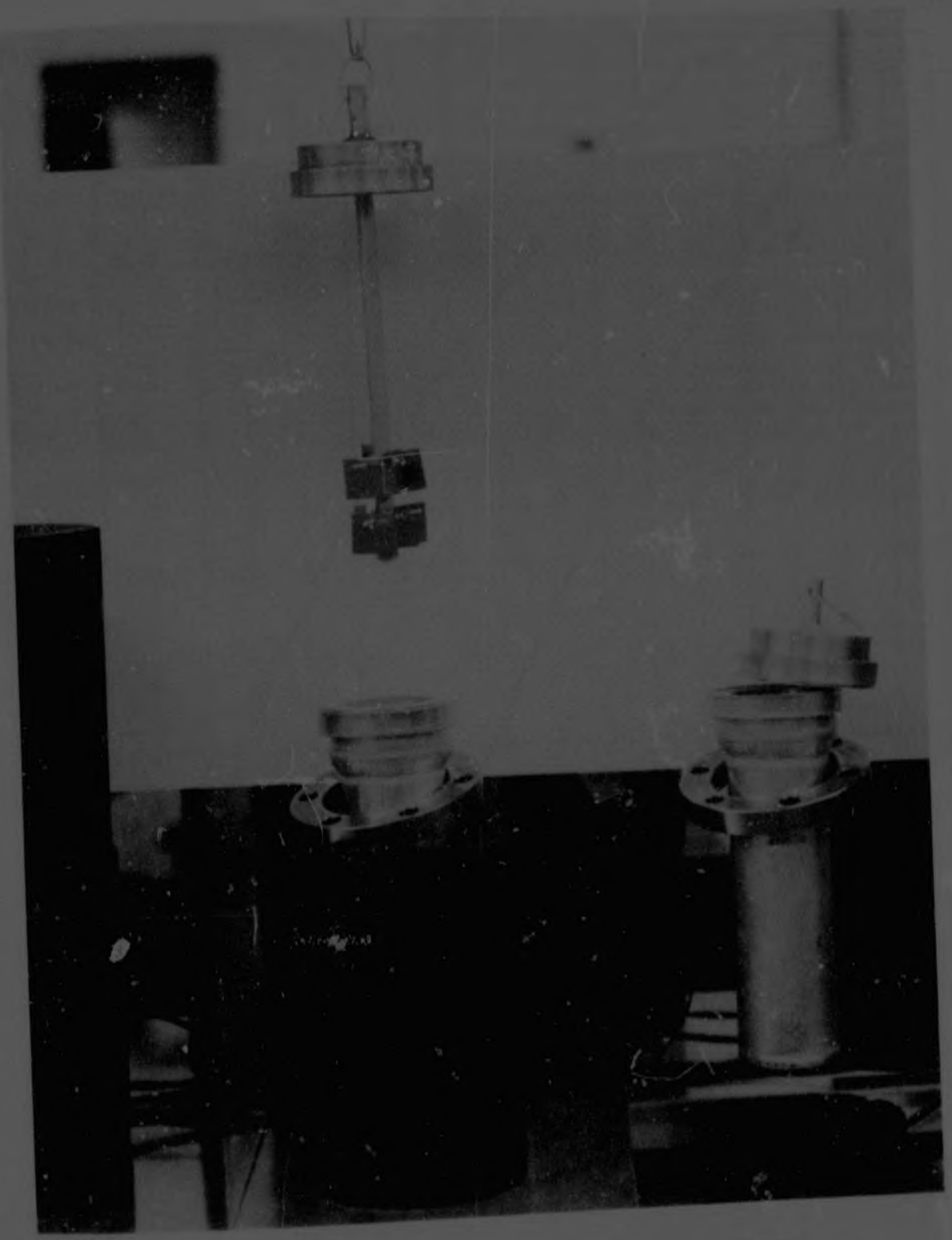

FIGURE 3.16 : DETAIL OF CORROSION CHAMBER

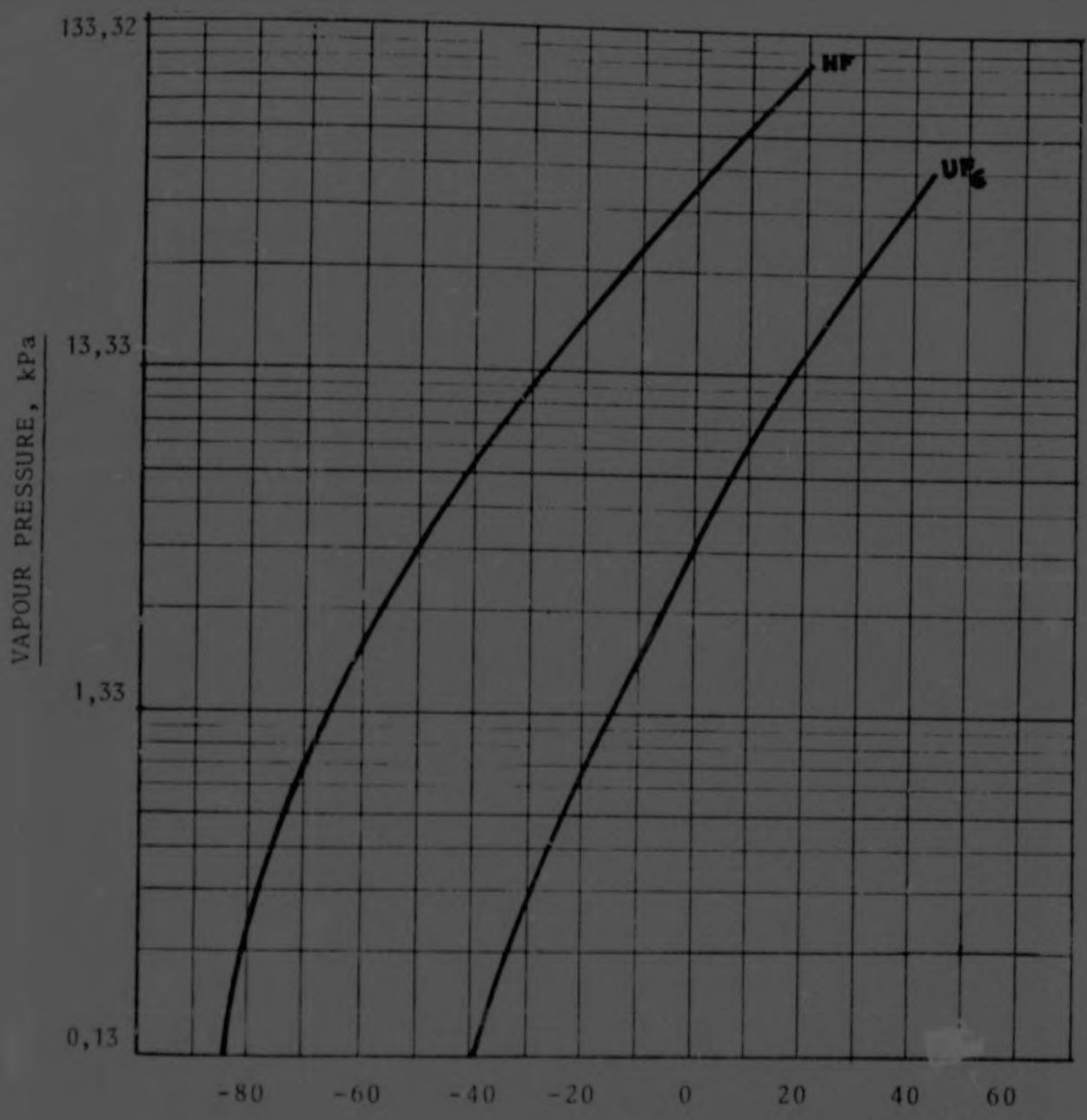

FIGURE 3.17 : VAPOUR PRESSURES OF HF AND UF_6

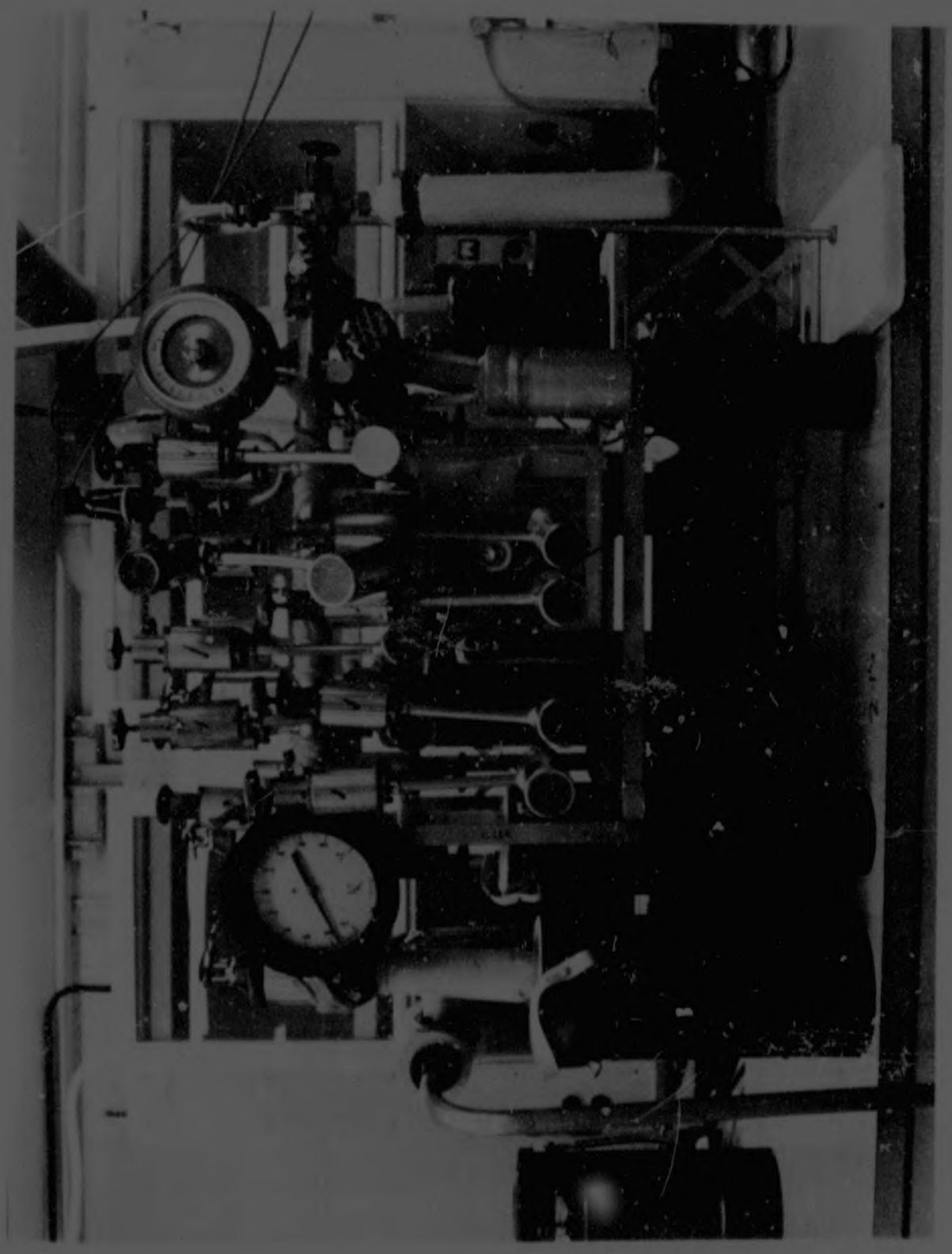

FIGURE 3.18 : EQUIPMENT FOR HANDLING UF_6 GAS

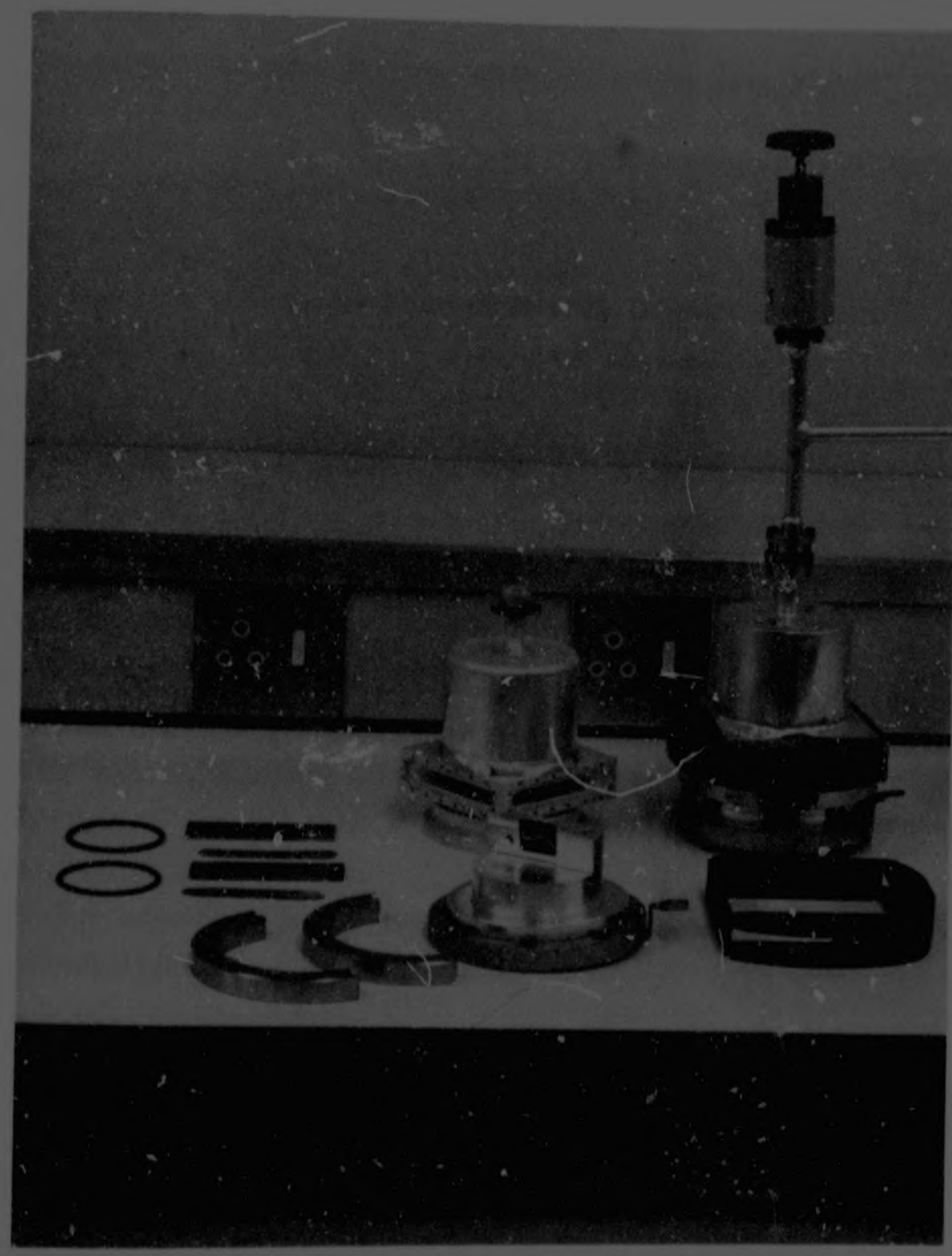

FIGURE 3.19 : EQUIPMENT USED FOR IN SITU X-RAY ANALYSIS OF CORRODING SURFACES

4. RESULTS AND DISCUSSION

4.1 Introduction

The gains in mass for the different alloys investigated are summarized in table 4.1. The results were fitted to the power law

$$\Delta m = At^n \qquad (1)$$

which was chosen in view of its general nature. The values of the constants A and n for the different alloys and temperatures are summarized in table 4.2.

As inferred earlier, there are many parallels between fluorination by fluorinating gases such as UF_6, and dry oxidation. In the following discussion "oxidation" will be assumed to include "fluorination" unless an aspect is under consideration that merits taking cognisance of the special nature of UF_6.

4.2 Kinetics of Corrosion Processes

A study of the progress of a corrosion reaction as a function of time is one of the most important tools in the study of corrosion mechanisms. It must be added, however, that further information is invariably required before complete understanding of a particular corrosion system results.

The rates of many heterogeneous oxidation reactions are controlled by (a) chemical reaction including adsorption at the gas/solid interface or (b) steady state diffusion of the active species through the solid reaction products.These two processes can be described by the following isothermal rate equations

$$\frac{d(\Delta m)}{dt} = k_\ell . \qquad (2)$$

and

$$\frac{d(\Delta m)}{dt} = \frac{k_p}{\Delta m} \qquad (3)$$

where Δm represents the mass increase per unit area, t time and k_ℓ and k_p the linear and parabolic rate constants respectively. These two equations in their integrated form provide linear and parabolic plots of mass increase with time respectively. Most of the remaining reactions comply with logarithmic, inverse logarithmic or asymptotic behaviour with respect to the Δm vs.t plot.

Reference to table 4.2 reveals that the values of n found in this investigation rarely exceeded 0,5. A value of 0,5 would signify a thermal diffusion process as the rate-determining step. Such a process may include a uniform diffusion of one or both reacting species through a dense scale (Wagner mechanism) or a uniform diffusion of gas into the metal. As UF_6 corrosion of copper alloys was in most instances accompanied by the deposition of solid uranium reaction products on the surface, which forms as a result of reactions of the type

$$UF_6 \longrightarrow UF_{6-x} + x\,F^- \qquad (4)$$

the second possibility seems less likely.

Table 4.2 also indicates that values of n lying between 0,5 and 0,33 occur frequently. Kofstad [1] states that oxidation reactions are frequently found to follow a combination of rate laws. This may mean either that the oxidation occurs by two simul-

[1] Per Kofstad, "High Temperature Oxidation of Metals," John Wiley & Sons, Inc. (1966), p.14

taneous mechanisms, one of which predominates during the initial stages and the other after extended oxidation, or that changes may take place in the rate-determining mechanism as the result of changes in the nature of the oxide scale. In equations such as

$$x^m = k_m t + C_m \qquad (5)$$

when m has a value of 3 or 4, the rate equations are termed cubic and quartic, respectively. Such rate equations may arise, for instance, if the total oxidation comprises two processes : one logarithmic and the other parabolic. Equation (5) is also frequently observed to apply over limited time periods in high-temperature oxidation of alloys for which the composition of the oxide scale changes with time.

It is therefore clear that, although the value of n could indicate the predominance of a specific reaction mechanism, the final answer can only be obtained by extensive research into the exact nature of the chemical reactions occurring, including the ionic species involved, and the physical nature of the solid corrosion products.

4.3 The Temperature Dependence of Oxidation Reactions

Arrhenius formulated his well-known equation in 1899. This equation can be written for the case of a unimolecular reaction :

$$\text{Reaction Rate} = \frac{dP}{dt} = K' e^{-Q/RT} \cdot P^n \qquad (6)$$

where K' is a constant, Q the activation energy, R the gas constant, T the absolute temperature, t time and P the concentration, i.e. the

amount of substance still available for the reaction. "n" determines the effect of the residual amount of substance on the reaction rate.

The Arrhenius equation is firmly established in the study of homogeneous kinetics, where its evaluation takes place isothermally, that is, by observing the fall in reaction rate with declining concentration P.

If the Arrhenius equation is applied to heterogeneous kinetics, some concepts have to be redefined. The term "concentration", used in homogeneous kinetics, cannot be transferred to heterogeneous kinetics since it becomes meaningless with pure solids. Concepts such as "activated complexes" and the "collision theory" are also difficult to reconcile with solid state reactions. A further major theoretical problem is presented by the pre-exponential factor K' and the activation energy Q, when these quantities are related to the physical situation. Q may be complexly composed of several activation energies, with the possibility that the different contributions may vary with time. In the Wagner treatment of parabolic oxidation the parabolic rate constant is expressed in terms of electrical conductivity, transport numbers and diffusion coefficients. For other reaction mechanisms correlation with physical properties of the reacting metals, oxides and gases is much more difficult.

As a rule it may be stated that the activation energy remains constant as long as the same rate-determining mechanism prevails.

4.3.1 Determining the Activation Energy of Non-Linear Corrosion Reactions

As was indicated, the corrosion of copper alloys in gaseous

UF_6 can be represented by the equation

$$\Delta m = At^n \tag{7}$$

The corrosion rate at any given moment is

$$\frac{d(\Delta m)}{dt} = n\,At^{n-1} \tag{8}$$

The rate of any thermally activated process is given by the Arrhenius equation

$$\frac{d(\Delta m)}{dt} = K.e^{-Q/RT} \tag{9}$$

Non-linear reactions display a time-dependent rate with the result that, in equation (9), either K or Q must be time-dependent. As this condition cannot apply to Q generally it follows that

$$K = f(t) \tag{10}$$

The time dependence of K is unknown, but if it can be assumed that it is of the form

$$K = Ct^m \tag{11}$$

we can write

$$\frac{d\Delta m}{dt} = Ct^m \,.\, e^{-Q/RT} \tag{12}$$

Comparing equation (12) with equation (8), we obtain

$$m + 1 = n \tag{13}$$

and

$$An = Ce^{-Q/RT} \tag{14}$$

which on taking logarithms gives

$$\ell n\ An = \ell n C - Q/RT \qquad (15)$$

Equation (15) gives a straight line when ℓn An is plotted against $\frac{1}{T}$ and the slope gives the value of $-\frac{Q}{R}$.

4.4 X-ray Diffraction of Corroded Specimens

A number of corroded specimens were examined by means of X-ray diffraction, using the techniques described in section 3.6.4. The results are summarized in tables 4.3 and 4.4.

The information recorded in table 4.4 was obtained from two groups of specimens. The first group had been given a pre-fluorination treatment in UF_6 at 50 °C for 140 h and were then corroded at 150 °C and 80 °C during the course of the experiment. In the second group of specimens, the temperature was initially kept at 80 °C for 600 h and then suddenly increased to 150 °C. The X-ray results therefore relate to the way in which the uranium fluorides formed initially, to their reaction with the UF_6 gas in the second part of the experiment, and to the occurrence of further corrosion.

Reference to the Agron-diagram (figure 1.2) and tables 4.3 and 4.4 leads to the conclusion that the nature of the uranium subfluoride formed in the corrosion reaction is dictated by the substrate. Very reactive metals give rise to U_2F_9 at temperatures much lower than expected from the Agron-diagram. Thermodynamic considerations would, however, require the presence of the equilibrium constituent at the gas/corrosion product interface. This constituent may be present as an extremely thin layer and therefore cannot be detected by the X-rays. There is, however, no experimental support for this statement.

The results summarized in table 4.4 are interesting in that the presence of α-UF_5 is indicated in experiments in which the temperature was lowered from 150 to 80 °C. This α-UF_5 is derived from U_2F_9 as a result of its reaction with UF_6:

$$U_2F_9(s) + UF_6(g) \longrightarrow 3\ \alpha\text{-}UF_5(s)$$

The fact that α-UF_5, and not β-UF_5 is formed (as would be expected from the Agron diagram) is in accordance with the results of Barberi and Hartmanshenn [2] who showed that the α-UF_5 ⟶ β-UF_5 transformation did not occur.

The fact that both U_2F_9 and α-UF_5 were formed on the Muntz metal specimen (table 4.4, figure 4.32) indicates that the initial β-UF_5 formed at 80 °C had been transformed to α-UF_5 at 150 °C with further corrosion at 150 °C leading to U_2F_9.

Figure 4.1 shows a surface which, before exposure to air, indicated the presence of β-UF_5. Figure 4.2 is a micrograph of U_2F_9-crystals on 70/30 brass. U_2F_9, although less sensitive to moisture than β-UF_5, is slowly disintegrated by virtue of the reaction

$$2\ U_2F_9 + 2\ H_2O \longrightarrow 3\ UF_4 + UO_2F_2 + 4\ HF$$

In the micrograph, crystals can be identified which have undergone this transformation.

4.5 Corrosion of the Copper-Zinc Alloys

Figure 4.3 illustrates the corrosion behaviour of 70/30 brass in 15 kPa UF_6 at different temperatures. The values of n (see table 4.2), ranging from 0,55 to 0,41, indicate that the

---

2) P. Barberi and O. Hartmanshenn, "The Microcalorimetric Study of the UF_4-UF_6 System," ANL-TRANS 654 (CEA-N-916)

corrosion products have a stifling effect on the corrosion process. As indicated in section 4.4 these products consisted mainly of β-UF_5 at the lower temperatures and U_2F_9 at the higher temperatures.

Figures 4.4 to 4.6, showing sections of α-brass specimens corroded at 150 ^{o}C, reveal penetration of the surface by the corroding medium, as well as a thick external scale comprising mainly U_2F_9. An Auger line scan (figure 4.8) along the line indicated in figure 4.7 shows high concentrations of both zinc and fluoride ion in the penetration zone. Fluoride ion penetration was difficult to detect at temperatures below 120 ^{o}C but cannot be ruled out. In alloys containing less than 15 % Zn the effect was never confirmed mainly as a result of the very thin corrosion layers formed on these alloys.

The conclusion can therefore be drawn that, in Cu-Zn alloys containing more than about 15 % Zn, fluoride ions penetrate the alloy at temperatures above 100 ^{o}C to precipitate ZnF_2. This process is accompanied by the diffusion of zinc atoms to the reaction zone. In figure 4.4 the dezincified zone is clearly demarcated by a line running parallel to the original specimen surface. The area between this line and the area of zinc fluoride precipitation is thought to contain mainly porous copper, voids being formed by the outward diffusion of zinc (see fig. 4.6) These processes are well known in conventional dezincification of brass by, for instance, chloride-containing water. It would appear, however, that the nature of the dezincification process is strongly dependent on the zinc content of the alloy in question. While, in the case of the Cu 15 Zn and Cu 20 Zn alloys, no zinc could be detected in

the external corrosion scale, electron microscopy revealed that, in the Cu 30 Zn alloy, a continuous layer of zinc fluoride existed below the uranium-containing outer scale. By bending a corroded specimen in order to crack the surface layers, the micrograph recorded in figure 4.9 was obtained.

Figure 4.10 shows that a similar situation is found in the 60 Cu 40 Zn alloy (Muntz metal). By studying corroded Muntz metal specimens in section it was found that de-alloying of α- and β-crystals occurred at the same rate and that no precipitation of zinc fluoride had occurred in the metal. Figure 4.11 shows a Muntz metal surface after 1000 h contact with UF_6 at 150 °C and partial removal of the corrosion layers. Viewing the removed layer from the underside, a zinc fluoride layer was found (figures 4.12 (area A) and 4.13) that appeared to replicate the roughness of the specimen surface. Figure 4.14 shows the X-ray fluorescence spectrum taken from area B in figure 4.12. Apart from the large uranium peak, small peaks due to copper and zinc are also apparent. Generally speaking, it can be stated that two well defined strata were found with a limited amount of interdiffusion.

Figure 4.15 shows the fluorescence spectrum originating from the bare surface (area C) in figure 4.11. Enrichment in copper due to the outward diffusion of zinc is evident.

Figure 4.16 indicates the influence of the zinc content of copper-zinc alloys on the corrosion behaviour. There is a general tendency for the alloys to decrease in corrosion resistance from pure copper to about Cu 20 % Zn. From 20 to 40 % zinc the reactivity remains relatively constant, except at the higher temperatures where a decrease in corrosion resistance is again found.

From figure 4.17, it can be seen that copper-zinc alloys display a break in the log rate against $\frac{1}{T}$ plots, which indicates a change in mechanism. It is significant that the change in mechanism shifts to lower temperatures as the zinc content of the alloy is increased. By referring to table 4.3 it would appear as if the change in mechanism can also be correlated with a change in the uranium fluoride detected in the corrosion layers.

The activation energies for the four alloys considered in figure 4.17 were calculated from the slopes of the curves and are reported in table 4.5. It appears that there is a marked drop in activation energy for the high-temperature reactions from 54,0 to 37,3 kJ mol^{-1} on increasing the zinc content from 5 % to 20 %. In the low-temperature region the activation energies were extremely low compared to values generally reported for oxidation reactions and probably relate to the relative ease with which fluoride ions can detach themselves from UF_6 molecules.

4.6 Corrosion of Copper-Zinc-Tin Alloys

Reference to tables 4.1.8 and 4.1.13 indicates that the addition of about 1 % tin drastically lowers the corrosion resistance of the α-β alloys. Figure 4.18 shows the surface of a specimen corroded at 80 °C for 188 h. The nodules are thought to be badly crystallized U_2F_9 embedded in a continuous layer of β-UF_5. Figure 4.19 shows that at the lower corrosion temperatures (below 100 °C) β-grains are not selectively attacked.

At 120 and 150 °C selective attack on the β-grains was observed. This is shown in figures 4.20 and 4.21. The exact area shown in figure 4.21 was located in the Auger-microprobe (figure 4.22)

and a line scan conducted as shown in figures 4.23 to 4.25 to detect variations in fluoride ion, zinc and copper concentrations. Precipitation of zinc fluoride in the β-phase, with virtually no attack on the α-phase, was apparent. Figure 4.26 illustrates the difference in attack experienced by the two phases. Attempts to detect differences in concentration of tin in the two phases were inconclusive due to the low percentage of tin in the alloy.

Admiralty brass, containing 0,3 % tin, displayed somewhat better corrosion resistance than the 70/30 brass. No fluoride penetration zone could be observed, and a continuous external layer of ZnF_2 was not detected. It is possible that ZnF_2 was precipitated in a diffuse zone as submicroscopic particles.

4.7 Corrosion of Copper-Tin Alloys

The 90/10 phosphor bronze displayed higher corrosion rates than the 95/5 alloy. This behaviour contrasts with that of copper-tin alloys in oxygen where it is found that an increase in the tin content leads to lower oxidation rates, as is indicated in figure 4.31. No internal fluorination was evident in these alloys.

4.8 Aluminium Bronze, Beryllium Copper and 18 % Nickel Silver

Aluminium bronze displayed exceptional stability in UF_6 gas. This behaviour could be due to the presence of a thin impervious layer of Al_2O_3 on the alloy surface. This layer will not be reduced by the hydrogen pretreatment at 150 ^{o}C. Thermodynamically, Al_2O_3 is more stable than AlF_3, thereby excluding attack by UF_6.

In the case of beryllium copper, beryllium oxide could likewise render protection when present as a thin continuous film. Further work is, however, required in order to elucidate the exact rôle of thin surface films.

Nickel silver performed satisfactorily at the lower temperatures, but the corrosion rate increased rapidly above 100 °C.

4.9 Corrosion of Pre-Oxidized Cu-Zn Alloys

The corrosion figures for the pre-oxidized alloys are reported in table 4.9 and the values of the constants A and n in table 4.10. The improvement in corrosion resistance resulting from pre-oxidation is shown graphically in figure 4.33. At 150 °C pre-oxidation improved the corrosion resistance of alloys containing more than 15 % zinc. Below this concentration the effect of oxidation was less obvious at 150 °C, although improvement was observed at the lower corrosion temperatures. This behaviour may relate to the different types of oxide formed on low and high zinc content brasses. Furthermore, photo-potential measurements on oxidized Cu-Zn alloys[3] indicate a continuous change from a predominantly p-type oxide on electrolytic copper to a predominantly n-type oxide on Muntz metal. It is known [4] that the semi-conducting properties of surface oxides can influence corrosion phenomena dramatically, but this aspect requires further study as far as UF_6 corrosion is concerned.

The activation energies for the corrosion of the oxidized alloys are reported in table 4.11. In comparison with the corresponding data in table 4.5, it appears that pre-oxidation at 150 °C increases the activation energy considerably.

---

3) S.W. Vorster, unpublished results

4) G. Bianchi et al., Corr. Sci, 12, 495-502 (1972)

4.10 Results of the Temperature-Change Experiments

The results of the temperature-change experiments are summarized in tables 4.6 and 4.7 and some data are displayed graphically in figures 4.27 to 4.29. In this type of experiment the "manometric technique" was employed to detect loss of UF_6 from the gas phase. The nature of the technique may explain the apparent drop in Δm subsequent to the lowering of the temperature from 150 ^{o}C to 80 ^{o}C at t = 500 h (fig. 4.27). The lower temperature will lead to more adsorbed UF_6 on the walls of the container, leading to a somewhat lower pressure reading. This effect was especially obvious in the Cu30Zn alloy in which the heavily corroded surface contributed substantially to the total area available for adsorption.

From figure 4.27 it would appear as if corrosion at 80 ^{o}C after the initial contact with UF_6 at 50 and 150 ^{o}C is virtually zero. A small UF_6 loss due to the slow reaction between U_2F_9 and UF_6 is possible. The initial "pre-fluorination" at 50 ^{o}C had a remarkable passivating effect on all the alloys studied as can be seen by comparing appropriate results in tables 4.1 and 4.6 for corrosion at 150 ^{o}C. It appears that the rates found after "pre-fluorination" are frequently less than one third of those found without this treatment.

On increasing the corrosion temperature from 80 ^{o}C to 150 ^{o}C the corrosion rate is increased considerably as is shown

graphically for three alloys in figure 4.28. A rough estimate of the activation energies for the processes involved in the tempera= ture range 80 - 150 ^{o}C can be made by assuming linear reaction kinetics at the two temperatures considered, and by employing the expression

$$Q = 8,314 \frac{T_1 T_2}{T_2 - T_1} \ln {}^{R_2}/_{R_1}$$

where Q represents the apparent activation energy and T_1 and T_2 the temperatures at which rates R_1 and R_2 were determined respec= tively.

For 80 and 150 ^{o}C this simplifies to

$$Q = 17,7 \ln {}^{R_2}/_{R_1} \text{ kJ mol}^{-1}$$

The apparent activation energies thus obtained are contained in table 4.8. These values are very much lower than values reported in table 4.5 and probably relate to the reactions between UF_6 and fluorides present on the surfaces and not to the corrosion reactions.

4.11 Discussion

The effects observed in the Cu-Zn and Cu-Zn-Sn alloys merit further discussion. As was reported in sections 4.5 and 4.6, zinc fluoride is formed internally in the alloys containing less than about 20 % Zn and externally in alloys containing 30 and 40 % Zn. Furthermore, this effect is reversed by the addition of about 1 % Sn, but in naval brass the ß-phase is attacked preferentially.

The free energies of formation for CuF_2 and ZnF_2 indicate that the latter compound will always form preferentially in copper zinc alloys. The following values have been published[5]:

$$\Delta F^{o}_{298}\ (ZnF_2) = -757\ kJ\ mol^{-1}$$

$$\Delta F^{o}_{298}\ (CuF_2) = -563\ kJ\ mol^{-1}$$

In the reaction of UF_6 with Cu-Zn alloys, the transport of zinc atoms to the reaction zone therefore seems to be vitally important. This phenomenon is also relevant in stress-corrosion, high-temperature oxidation (including internal oxidation) and de-alloying studies of Cu-Zn alloys.

Rhines and Mehl[6] determined the diffusion activation energy of various binary copper alloys including Cu-Zn alloys. Figure 4.30 shows the relationship between Q and the concentrations for the different systems. For the Cu-Zn system it is significant that a sudden drop in Q was observed for zinc concentrations between 10 and 15 atomic percentage. Figure 4.31[7] illustrates the increase in oxidation resistance in alloys containing more than about 15 mass percentage zinc. In a study of brass sulphidation Nowak et al.[8]

---

5) O. Kubaschewski and E.L.L. Evans, "Metallurgical Thermochemistry", Pergamon Press (1958)

6) F.N. Rhines and R.F. Mehl, Trans. A.I.M.E. 128, 185-222 (1938)

7) O. Kubaschewski and B.E. Hopkins, "Oxidation of Metals and Alloys," Butterwoths (1962) p. 250

8) J.F. Nowak, M. Lambertin and J.C. Colson, Corr. Sci., 17, 603-617 (1977)

found that with low Zn brasses a thin, continuous, Cu_2S layer formed initially which grew by outward cation migration of copper. With a high Zn content (40 %) the zinc completely sulphidized before copper was attacked. ZnS formed externally, which led to lower reaction rates. Various studies of the high temperature oxidation behaviour of brasses have been undertaken[9, 10]. Parabolic oxidation of CuZn alloys has been found at 800 °C when the zinc content is 10 % or less. The protective scale was mainly Cu_2O. Above 20 % Zn the oxidation rate was not very sensitive to zinc content and mainly ZnO formed. Between 10 % and 20 % Zn the oxidation rate decreased sharply with increasing Zn concentrations, displaying non-parabolic oxidation kinetics due to changes in the protective scale.

Wagner[11] made a theoretical analysis of diffusion processes determining the oxidation rate of alloys. Wagner could predict that exclusive formation of ZnO would occur for alloys with a mole fraction of zinc above 0,15, which was in good agreement with Dunn's results[9].

It is therefore clear that Zn movement constitutes a key factor in the high-temperature behaviour of brasses in oxidizing atmospheres. In the present investigation, this is doubtless also true, as can be seen by comparing figures 4.30 and 4.16.

---

9) J.S. Dunn, J. Inst. Metals, 46, 25 (1931)

10) F.N. Rhines and B.J. Nelson, Trans. A.I.M.E. 156, 171 (1944)

11) C. Wagner, J. Electrochem. Soc., 99, 369 (1952)

In UF_6, however, increased Zn content leads to higher reactivity, from which it may be concluded that the formation of a continuous fluoride layer does not lead to the measure of protection of the substrate which is found with a continuous layer of ZnO. This may reflect on the relative ease with which fluoride ions can diffuse through ZnF_2, compared to the blocking effect of ZnO for oxygen ions.

As the diffusion of zinc atoms is enhanced in alloys containing more than 15 - 20 % Zn, and in view of the apparent ease with which fluoride ions can reach the metal surface, a maximum corrosion rate is to be expected when the zinc diffusion facilitates reactions at the outer surface of the alloy.

The exact role of Sn in the abovementioned processes is not clear. Some workers[12] are of the opinion that (additions increase the resistance of β-brasses to stress-corrosion cracking, but that the effect of tin is explicable in terms of its effect upon surface films rather than its effect on the stacking fault energy. In the present investigation no direct information regarding the rôle of tin was found, but the fact that the formation of an external layer of ZnF_2 at 150 ^{o}C is prevented by the addition of 1 % tin points towards its interference with the diffusion of zinc in α - β brasses.

---

[12] B.C. Synett and R.N. Parkins, Corr. Sci. 7, 597-605, (1967)

4.12 Summary and Conclusions

4.12.1 The corrosion behaviour of nineteen copper alloys in gaseous UF_6 at a pressure of 15 kPa has been investigated. Corrosion/time relationships were established at five temperatures ranging from 50 to 150 ^{o}C and for exposure times between 5 and 1 000 h.

4.12.2 Post-corrosion studies of surface layers were undertaken, employing X-ray diffraction analysis, X-ray fluorescence analysis and Auger spectroscopy. By taking special precautions the uranium-containing corrosion products could be identified and penetration zones could be studied in carefully prepared sections of specimens.

4.12.3 Arrhenius plots of corrosion rates in the temperature range studied revealed changes in reaction mechanism which coincided with changes in the intermediate uranium fluoride present. X-ray investigations of corroded surfaces of the 90Cu10Zn alloy indicated the presence of β-UF_5 after exposure to UF_6 in the temperature range 50 to 120 ^{o}C. Reactions of the type

$$M(s) + 2\ UF_6(g) \rightarrow MF_2(s) + 2\beta\text{-}UF_5(s)$$

(where M signifies the corroding metal) therefore occur. At 150 ^{o}C U_2F_9 was detected, suggesting reactions of the type

$$3M(s) + 4UF_6(g) \rightarrow 3MF_2(s) + 2U_2F_9(s)$$

A corresponding change in the slope of the reaction rate/reciprocal temperature plot was observed, implying a change in reaction mechanism. The change in mechanism shifted to lower temperatures as the reactivity of alloys in a particular alloy system increased,

as exemplified by the copper-zinc system. Addition of zinc to copper in the concentration range 0 to 40 mass percentage led to a decrease in corrosion resistance and a lowering of the temperature at which U_2F_9 was formed. Most of the alloys studied displayed breaks in their Arrhenius plots.

The corrosion reactions can be split into the partial reactions

$$UF_6(ads) + xe^- \rightarrow UF_{(6-x)}^{x+} + xF^-$$

and

$$xM \rightarrow xM^+ + xe^-$$

It follows that the electronic and ionic conductivities of the corrosion products are important in determining the corrosion resistance of a particular alloy. There are indications that the intermediate uranium fluorides are non-stoichiometric compounds (Chapter 1 ref. 6). In this respect U_2F_9 is of particular interest as it contains uranium in both the +4 and +5 oxidation states. Those non-stoichiometric compounds which are metal-deficient are also semi-conductors. Under a potential difference an electron can switch from an ion in the lower oxidation state to an ion in the higher oxidation state, thus constituting a current. As an electron moves across the crystal in one direction, a metal ion in the higher oxidation state appears to move in the opposite direction. It can therefore be reasoned that the partial reaction involving diffusion of fluoride ions should be the rate-determining step in those instances where U_2F_9 is the intermediate fluoride present. This would imply parabolic reaction kinetics:

$$\Delta m = At^n \qquad \text{with } n = 0,5.$$

The results were not very conclusive in this respec but it can be stated generally that values of n lying between 0,4 and 0,5 were frequently found in the higher temperature range and with the less resistant alloys, while lower values of n resulted when β-uranium pentafluoride formed.

4.12.4 This research revealed that the Agron diagram has limited value in predicting the nature of the intermediate uranium fluorides resulting from reaction between copper alloys and uranium hexafluoride.

The temperat regions for the stability of the three intermediate fluorides encountered in this investigation are, according to the Agron diagram (for a UF_6 pressure of 10 kPa):-

β-UF_5	:	50 °C to 119 °C
α-UF_5	:	119 °C to 262 °C
U_2F_9	:	262 °C to 358 °C

With the possible exception of electrolytic copper corroding at 150 °C, α-uranium pentafluoride was never present as a result of a direct corrosion reaction. It always formed via U_2F_9 or β-UF_5 on changing the temperature. This phenomenon is further discussed in 4.12.5.2. With the less resistant alloys U_2F_9 was identified at temperatures as low as 80 °C (70/30 brass).

It is therefore clear that the occurrence of α-UF_5 and U_2F_9 cannot be accurately predicted with the aid of the Agron diagram. It is probably valid only when equilibrium exists between UF_6 and uranium fluorides in contact with an inert supporting surface. Thermodynamic considerations would require the presence of the equilibrium constituent at the gas/corrosion product interface, but this constituent may be present as an extremely thin layer and therefore unlikely to be detected by means of X-ray diffraction. β-UF_5 was never detected above 120 °C, which is in accordance with the Agron diagram.

4.12.5 An investigation into the effect of pre-fluorination of copper alloys on the subsequent corrosion reactions led to the following conclusions:

4.12.5.1 Pre-fluorination of copper-zinc alloys at 50 °C for 140 h led to corrosion rates at 150 °C which were lower by factors between 2 and 4 compared to corrosion rates found without pre-fluorination. The improvement resulting from pre-fluorination was less evident in brasses containing less than 15 % zinc and in electrolytic copper.

4.12.5.2 Investigations in which the reaction temperature was changed during the course of the experiments give information about the reactions that occurred between UF_6 and existing uranium fluorides. Electrolytic copper was exposed to UF_6 for 600 h at 80 °C, leading to the formation of β-UF_5. Continuation of the experiment at 150 °C resulted in the formation of a mixture of α- and β-UF_5, which suggests α-UF_5 as the primary

corrosion product and also that the allotropic transformation

$$\beta\text{-}UF_5 \rightarrow \alpha\text{-}UF_5$$

is very sluggish.

4.12.5.3 Exposure of 70/30 brass to UF_6 at 150 °C is known to lead to the formation of U_2F_9. On lowering the temperature from 150 °C to 80 °C a mixture of α-UF_5 and U_2F_9 was found. Partial disproportionation had occurred:-

$$U_2F_9 + UF_6 \rightleftarrows 3\ \alpha\text{-}UF_5.$$

The fact that α-UF_5 and not β-UF_5 was found (as would be expected from the Agron diagram) is in accordance with the results of other workers who found that the

$$\alpha\text{-}UF_5 \rightarrow \beta\text{-}UF_5$$

allotropic transformation did not occur. This effect was also observed with 95/5 brass, 80/20 brass and leaded brass.

4.12.5.4 Mixtures of U_2F_9 and β-UF_5 were produced on alloys exposed to UF_6 at temperatures near the temperatures where changes in mechanism were detected. This was found for leaded brass and 95/5 phosphor bronze at 100 °C and for 18 % nickel silver at 120 °C.

4.12.6 An internal fluorination zone was found in copper-zinc alloys containing less than 20 mass percentage zinc, following contact with UF_6 at temperatures above 100 °C. This zone is due primarily to the mobility of both zinc atoms and fluoride ions in the alloy, leading to the internal precipitation of ZnF_2.

4.12.7 The copper-zinc alloys containing more than about 20 mass percentage of zinc were more reactive towards UF_6 and formed a continuous external layer of zinc fluoride, covered by a layer of intermediate uranium fluorides. The outward diffusion of zinc leads to the formation of internal voids.

From the literature it is known that the activation energy for zinc diffusion is much lower in alloys containing more than about 10 atom percentage zinc.

4.12.8 The α-β copper-zinc alloy containing tin (Naval brass) suffered selective attack of the β-phase by UF_6 at temperatures above 100 ^{o}C. The tin-containing α-brass (Admiralty brass) corroded at a lower rate than the corresponding tin-free alloy.

4.12.9 Aluminium bronze was exceptionally stable in UF_6 gas. The existence of a thin continuous layer of air-formed Al_2O_3 could explain this behaviour. A similar mechanism may apply to beryllium copper.

4.12.10 UF_6-corrosion activation energies for copper alloys are comparatively low, ranging from 12,8 to 54 kJ mol^{-1}. Figures of 70 to 91 kJ mol^{-1} are normally found for low temperature oxidation of metals.

4.12.11 Pre-oxidation of copper-zinc alloys (15 minutes at 150 ^{o}C) enhanced their resistance to UF_6 attack. UF_6-corrosion activation energies increased considerably, varying from 38 kJ mol^{-1} to 103 kJ mol^{-1}.

Pre-oxidation improved UF_6 corrosion resistance at 150 ^{o}C of alloys containing more than 15 weight percentage zinc. Below this zinc concentration the effect of oxidation was less obvious at 150 ^{o}C, although improvement was observed at the lower corrosion temperatures. This behaviour probably relates to the different types of oxide formed on low and high zinc content brasses. It is possible that the oxidation of the low zinc content brasses led to predominantly copper oxide while the more impermeable ZnO formed on zinc-rich alloys. Thermodynamically both Cu_2O and ZnO will be unstable in UF_6-gas, but the reaction kinetics are probably unfavourable for the destruction of these oxides, except at 150 ^{o}C (and above) for Cu_2O.

4.12.12 The parallel that is drawn by some French workers between UF_6 corrosion and dry corrosion in oxygen (Chapter 2, references 11, 13) has been found to be of little value, especially with regard to the copper-zinc and the copper-tin systems. Both tin and zinc additions to copper are found to increase the oxidation resistance of the alloys. In UF_6, however, it was found that increased tin and zinc contents lead to higher reactivity. It may therefore be concluded that the formation of a continuous fluoride layer (which was observed) does not afford protection to UF_6 as is found with ZnO (or SnO) layers in oxygen. The similarity between UF_6 corrosion and dry oxidation is therefore very superficial, especially in view of the solid reaction products which are deposited on the surface of the corroding metal. These deposits influence the corrosion process in a unique way, as they frequently react with the corroding medium. These effects are mostly absent in conventional oxidation.

TABLE 4.1 : CORROSION FIGURES FOR COPPER ALLOYS EXPOSED TO UF_6 GAS AT 15 kPa

TABLE 4.1.1 : ELECTROLYTIC Cu

Temperature ^{o}C	Exposure Time t, h	Mass Increase Δm, $\mu g\ cm^{-2}$
50	5	24
	18	20
	48	22
	185	46
	984	42
80	5	30
	23	44
	42	80
	188	127
	1026	224
100	5	60
	20	44
	41	68
	163	162
	979	278
120	3	71
	21	104
	43	136
	187	222
	1005	222
150	5	154
	16	247
	41	514
	209	791
	1006	1392

CORROSION FIGURES FOR COPPER ALLOYS EXPOSED TO UF_6 GAS AT 15 kPa

TABLE 4.1.2 : 95/5 BRASS

Temperature ^{o}C	Exposure Time t, h	Mass Increase Δm, $\mu g\ cm^{-2}$
50	5	19
	18	27
	48	29
	185	69
	984	54
80	5	37
	23	36
	42	106
	188	108
	1026	256
100	5	53
	20	47
	41	89
	163	192
	979	328
120	3	69
	21	115
	43	152
	187	295
	1005	507
150	5	194
	15	287
	16	361
	41	601
	209	947
	1006	1662

CORROSION FIGURES FOR COPPER ALLOYS EXPOSED TO UF_6 GAS AT 15 kPa

TABLE 4.1.3 : 90/10 BRASS

Temperature ^{o}C	Exposure Time t, h	Mass Increase Δm, $\mu g\ cm^{-2}$
50	5	20
	18	16
	48	42
	185	94
	984	106
80	5	36
	23	56
	42	124
	188	230
	1026	463
100	5	74
	20	73
	41	162
	63	287
	979	565
120	3	141
	21	170
	43	250
	187	488
	1005	937
150	5	272
	16	555
	41	910
	209	1563
	1006	3074

CORROSION FIGURES FOR COPPER ALLOYS EXPOSED TO UF_6 GAS AT 15 kPa

TABLE 4.1.4 : 85/15 BRASS

Temperature ^{o}C	Exposure Time t, h	Mass Increase Δm, $\mu g\ cm^{-2}$
50	5	22
	18	48
	48	70
	185	106
	984	189
80	5	43
	23	35
	42	166
	188	434
	1026	830
100	5	70
	20	115
	41	255
	163	538
	979	1222
120	3	130
	21	346
	43	477
	187	927
	1005	693
150	5	335
	16	950
	41	1181
	209	2349
	1006	4854

CORROSION FIGURES FOR COPPER ALLOYS EXPOSED TO UF_6 GAS AT 15 kPa

TABLE 4.1.5 : 80/20 BRASS

Temperature ^{o}C	Exposure Time t, h	Mass Increase Δm, $\mu g\ cm^{-2}$
50	5	37
	18	47
	48	81
	185	164
	984	321
80	5	62
	23	50
	42	219
	188	627
	1026	1224
100	5	114
	20	170
	41	415
	163	778
	979	1548
120	3	177
	21	493
	43	650
	197	1278
	1005	2102
150	5	290
	16	1288
	41	1615
	209	3037
	1006	5635

CORROSION FIGURES FOR COPPER ALLOYS EXPOSED TO UF_6 GAS AT 15 kPa

TABLE 4.1.6 : 70/30 BRASS

Temperature ^{o}C	Exposure Time t, h	Mass Increase Δm, $\mu g\ cm^{-2}$
50	5	28
	18	69
	48	59
	185	245
	984	331
80	5	56
	23	41
	42	380
	188	641
	1026	1213
100	5	208
	20	227
	41	328
	163	698
	979	1550
120	3	114
	21	129
	43	701
	187	1218
	1005	1968
150	5	200
	16	899
	41	1559
	209	3441
	1006	6021

CORROSION FIGURES FOR COPPER ALLOYS EXPOSED TO UF_6 GAS AT 15 kPa

TABLE 4.1.7 : 70/30 BRASS (COMMERCIAL ALLOY)

Temperature ^{o}C	Exposure Time t, h	Mass Increase Δm, $\mu g\ cm^{-2}$
50	5	38
	18	94
	48	108
	185	256
	984	400
80	5	38
	23	45
	42	296
	188	516
	1026	1057
100	5	189
	20	123
	41	404
	163	759
	979	1509
120	3	296
	21	412
	43	682
	187	1143
	1005	2066
150	5	169
	15	1145
	41	1601
	209	3095
	1006	6045